Liver Tumors II: Malignant Tumors of the Liver

17

Naoshi Nishida, Ryuichi Kita, Kenichi Miyoshi, Masahiko Koda, Masaki Iwai, and Arief A. Suriawinata

Contents

Abbreviations

AFP	α-Fetoprotein
ARID1	AT-rich interactive domain-containing protein 1A
BCLC	Barcelona clinic liver cancer
CCC	Cholangiocellular carcinoma
CEUS	Contract-enhanced US
CK	Cytokeratin
CoCC	Cholangiolocellular carcinoma
CT	Computed tomography
CTA	CT arteriography
CTAP	CT arterial portography
EZH2	Zeste homolog 2
Gd-EOB-DTPA	Gadolinium-ethoxybenzyl-diethylenetriamine pentaacetic acid
Gd-EOB-MRI	Gd-EOB-DTPA-enhanced MRI
HAIC	Hepatic arterial infusion chemotherapy
HBV	Hepatitis B virus
HCC	Hepatocellular carcinoma
HCV	Hepatitis C virus
MRI	Magnetic resonance imaging
NEC	Neuroendocrine cancer
NEN	Neuroendocrine neoplasm

N. Nishida, MD, PhD (✉)
Osaka, Japan
e-mail: naoshi@med.kindai.ac.jp

R. Kita, MD, PhD
Osaka, Japan

K. Miyoshi, MD, PhD · M. Koda, MD, PhD
Tottori, Japan

M. Iwai, MD, PhD
Kyoto, Japan

A. A. Suriawinata, MD
New Hampshire, USA

E. Hashimoto et al. (eds.), *Diagnosis of Liver Disease*, https://doi.org/10.1007/978-981-13-6806-6_17

Table 17.1 Malignant tumor of the liver

Epithelial tumors	Hepatocellular	• Hepatocellular carcinoma
		• Hepatocellular carcinoma, fibrolamellar variants
		• Hepatoblastoma, epithelial variants
	Biliary	• Intrahepatic cholangiocarcinoma (cholangiocellular carcinoma)
		• Intraductal papillary neoplasm with an associated invasive carcinoma
		• Mucinous cystic neoplasm with an associated invasive carcinoma (mucinous cystadenocarcinoma)
	Mixed or uncertain origin	• Calcifying nested epithelial stromal tumor
		• Carcinosarcoma
		• Combined hepatocellular and cholangiocarcinoma
		• Hepatoblastoma, mixed epithelial-mesenchymal
		• Malignant rhabdoid tumor
Mesenchymal tumor	Vascular tumors	• Epithelioid hemangioendothelioma
		• Angiosarcoma
	Hematological tumor	• Malignant lymphoma
	Miscellaneous tumors	• Leiomyosarcoma
		• Rhabdomyosarcoma
		• Embryonal sarcoma (undifferentiated sarcoma)
		• Malignant fibrous histiocytoma
		• Malignant schwannoma
		• Hepatic liposarcoma
		• Kaposi sarcoma
		• Synovial sarcoma

Adapted from WHO classification of tumors of the liver and intrahepatic bile ducts (2010)

NET	Neuroendocrine tumor
OATP	Organic anion transporting polypeptide
PEI	Percutaneous ethanol injection
PIVKA-II	Prothrombin induced by vitamin K absence-II
PS	Performance status
PTC	Percutaneous transhepatic cholangiography
RFA	Radiofrequency ablation
SOL	Space-occupying lesion
TACE	Transarterial chemoembolization
TET1	Ten-eleven translocation methylcytosine dioxygenase 1
US	Ultrasonography

17.1 Definition and Classification

Primary liver tumors originate from hepatocytes, cholangiocytes, and mesenchymal cells (Table 17.1). Among liver tumors, hepatocellular carcinoma (HCC) is the most common; the majority of HCC develops as a result of chronic liver diseases that cause severe hepatocyte damage and regeneration. Chronic inflammation results in the formation of regenerative nodules as well as in the development of HCC through induction of many genetic/epigenetic alterations. Practitioners should attempt to differentiate HCC from benign and other malignant tumors and to treat it accordingly. Antiviral treatment for chronic hepatitis B (HBV) or C viruses (HCV) could reduce the risk of HCC emergence related to hepatitis virus [1, 2].

Cholangiocellular carcinoma (CCC) originates from intrahepatic or extrahepatic bile ducts and is the next most commonly encountered type of tumor after HCC. Recent whole-genome, epigenome, and transcriptome analysis revealed that there could be a molecular subtype in CCC that might reflect a difference of etiology. Cystadenocarcinoma is the malignant counterpart of bile duct cystadenoma. Hepatoblastoma is usually detected in children <2 years old, but a few cases in adolescents or young adults had been reported. Sarcomatous tumors are infrequently seen in the liver but angiosarcoma carries a grave prognosis.

17.2 Hepatocellular Carcinoma

HCC is a tumor with marked geographical variability in incidence, but both racial and genetic effects are of little importance in HCC. The relationship between HCC and chemicals, hormones, alcohol, nutrition, and the presence or absence of cirrhosis is complicated. Nevertheless, hepatitis B and C virus infection and aflatoxin exposure are significantly associated with the development of HCC [3, 4]. Therefore, it is important to follow patients chronically infected by HBV and HCV and exposed to aflatoxin by examining liver function tests, tumor markers, and image analysis. It is known that successful antiviral therapy could reduce the risk of HCC among patients with HBV and HCV infection [1, 2]. On the other hand, based on recent comprehensive genome and transcriptome analyses, a molecular classification of HCC that could relate to biological behavior of HCC has been proposed (Table 17.2).

Table 17.2 Classification of hepatocellular carcinoma based on transcriptome, genome, epigenome, and chromosomal alterations

Molecular feature	G1	G2	G3	G4	G5	G6
Alteration of cellular signaling based on the transcriptome analysis	Mitotic cell cycle			Wnt activation		
	AKT activation					
	Developmental and imprinting genes, IGF2		Cell cycle, nucleus pore		Stress and immune response	Amino acid metabolism, E-cadherin↓
Clinical feature	Woman. Africa, young, high AFP	Hemochromatosis				
	HBV-low copy number	HBV-high copy number				Satellite nodule
Methylation			CDKN2A		CHD1	
Mutation	AXIN1	TP53, AXIN1, PI3CA	TP53	HIF1A	CTNNB1	
Chromosomal status	Unstable			Stable		
Chromosomal alteration	4q, 16p, 16q	4q, 13q, 16p, 17p	4q, 5q, 16p, 17p, 21q, 22q			

Six HCC subgroups were determined through the unsupervised transcriptomic analysis by Boyault et al.; correspondence of the subgroups with their clinical characteristics as well as genetic, epigenetic, and chromosomal alterations were shown. (Boyault S et al. Transcriptome classification of HCC is related to gene alterations and to new therapeutic targets. Hepatology. 2007 Jan;45(1):42–52)

17.2.1 Etiology

Chronic HBV and HCV infections are the most frequent etiology of HCC. Other risk factors of HCC include alcoholic liver disease, nonalcoholic steatohepatitis, aflatoxin-B1 intake, diabetes, obesity, hereditary conditions, such as hemochromatosis, and metabolic disorders. Etiologies and risk factors of HCC vary by geographic locations.

17.2.2 Early HCC and Progressed HCC

It is well described that small HCC with less than 2 cm in diameter could be divided into two categories [5]: early and progressed HCCs. Early HCC is a small well-differentiated tumor with vaguely nodular appearance. On the other hand, progressed HCC is a mostly moderately differentiated tumor with distinct nodular appearance and microvascular invasion.

The histologic characteristics of early HCC include increased cell density more than two times of the surrounding liver, intratumoral portal tracts, pseudoglandular pattern, diffuse fatty change, and varying number of unpaired arteries. However, it is sometimes difficult to distinguish early HCC from high-grade dysplastic nodule, a premalignant lesion of HCC. The recognition of stromal invasion is the most important feature in differentiating early HCC from dysplastic nodule [5].

17.2.3 Diagnosis

The diagnosis of HCC is generally made by the increase of HCC-specific tumor markers, α-fetoprotein (AFP), AFP-L3, and prothrombin induced by vitamin K absence-II (PIVKA-II), and unique findings of diagnostic imaging [6–8]. Combination of measurement of serum AFP with PIVKA-II could increase the diagnostic accuracy of HCC.

During the development of HCC, several pathological changes are observed, such as increase of cellular density, decrease of portal vein flow, increase of arterial flow, and decrease of Kupffer cell. These pathological changes lead to the appearance of unique findings in imaging of HCC. Fibrous capsule and necrotic tissue are also detected in advanced tumor.

The findings of ultrasonography (US) image of HCC are as follows: mosaic pattern that reflects tumor heterogeneity, halo and lateral shadow that are associated with the presence of capsule, and nodule-in-nodule pattern that is attributed to multistep carcinogenesis of HCC [9, 10]. Portal vein and hepatic vein thromboses are also characteristic findings of HCC. Contract-enhanced US (CEUS) using perflubutane shows tumor stain at the early phase and defect in the Kupffer phase, because of the increase of arterial blood flow and decrease of Kupffer cell. Reperfusion defect in CEUS is one of the characteristic findings of HCC [11]. Dynamic computed tomography (CT) using multi-detector row CT is also used for the diagnosis of HCC; early vascular staining and washout of contrast agents at delayed phase are observed [12]. In advanced HCC, magnetic resonance imaging (MRI) is used to show low-intensity area and high-intensity area on T1-weighted image and T2-weighted image, respectively [13]. Gadolinium-ethoxybenzyl-diethylenetriamine pentaacetic acid (Gd-EOB-DTPA) is the most commonly used contrast medium for MRI diagnosis of HCC [14]. Gd-EOB-DTPA is incorporated into hepatocyte through the organic anion transporting polypeptide (OATP) transporter. Therefore, hepatobiliary phase of Gd-EOB-DTPA-enhanced MRI (Gd-EOB-MRI) shows defect in HCC because of the lack of OATP1B3 expression in the majority of HCC cells [15]. It is also known that a small subset of HCCs overexpressed OATP1B3 and showed increased uptake of Gd-EOB into tumor cells on hepato-

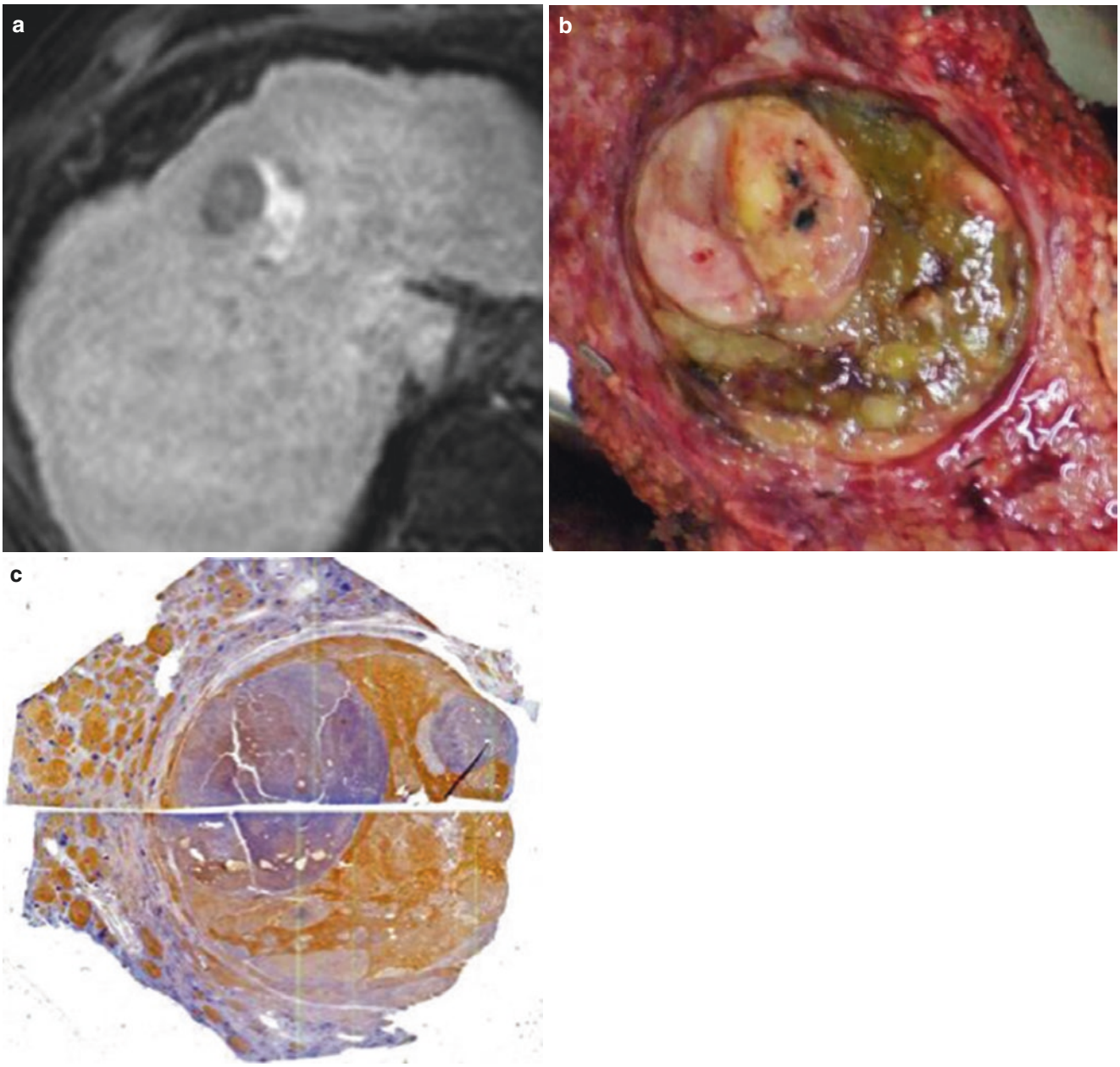

Fig. 17.1 Uptake of Gd-EOB-DTPA in the hepatobiliary phase of MRI in the tumor. The MRI image in the hepatobiliary phase of Gd-EOB-DTPA contract-enhanced MRI revealed high-intensity portion in the nodule (**a**). Macroscopic findings showed nodule-in-nodule pattern; the whitish nodule in green hepatoma with bile production ability (**b**). The loupe image of the tumor with OATP1B3 immunostaining (**c**). The region expressing OATP1B3 in the tumor corresponded to the green portion in the loupe image and the high-intensity portion with Gd-EOB-DTPA uptake in the hepatobiliary phase MRI image

biliary phase image (Figs. 17.1 and 17.2). Angiography of HCC reveals hypervascular tumor.

Case 17.1 (HCC Nodule with Uptake of Gd-EOB-DTPA) A 62-year-old male patient, who suffered from liver cirrhosis and hepatitis C virus infection, was referred to our hospital for further examination of the liver tumor. MRI examination revealed a 3 cm tumor in S4 with nodule-in-nodule pattern (Fig. 17.1). The region expressing OATP1B3 in the tumor corresponded to the portion with Gd-EOB-DTPA uptake in the hepatobiliary phase image (Figs. 17.1 and 17.2).

17.2.4 BCLC Staging System and Treatment of HCC

Barcelona Clinic Liver Cancer (BCLC) staging system is commonly applied for staging of HCC, which consists of five stages as follows [16]:

- Very early stage (0): tumor is less than 2 cm, performance status (PS) of the patient = 0, and Child-Pugh A.
- Early stage (A): a single tumor less than 5 cm or up to 3 tumors all less than 3 cm. PS 0 and Child-Pugh A or B.

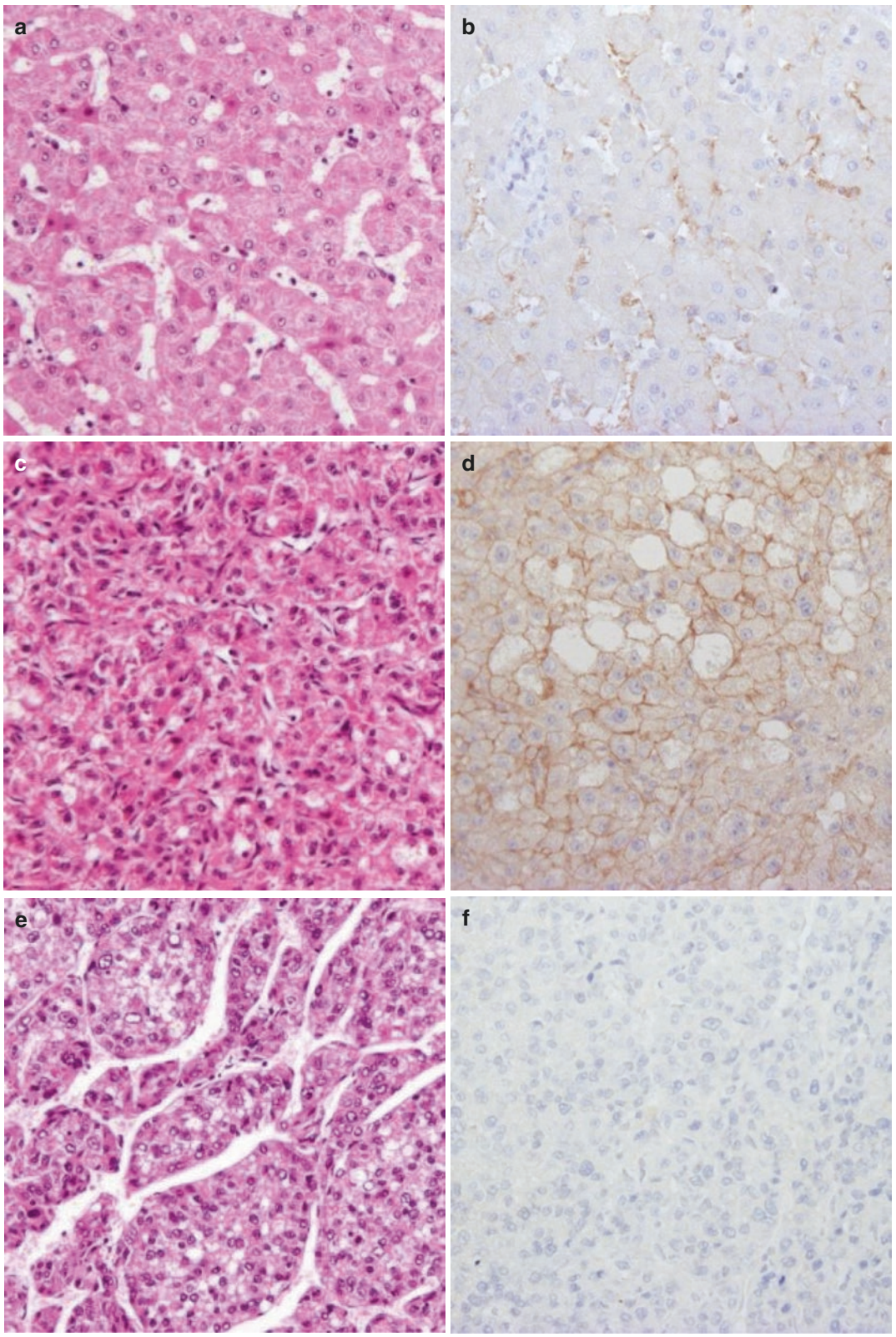

Fig. 17.2 Macroscopic images of surrounding noncancerous liver (**a**, **b**), the peripheral portion of HCC with Gd-EOB-DTPA uptake (**c**, **d**), and the central nodule without Gd-EOB-DTPA uptake (**e**, **f**). The images with HE staining (**a**, **c**, **e**) and immunohistochemical staining for OATP1B3 (**b**, **d**, **f**) are shown. Well- to moderately differentiated HCC in the peripheral portion of the tumor showed positive for membranous immunostaining of OATP1B3 on the cancer cells (**c**, **d**). Central tumor represents moderately differentiated HCC without expression of OATP8 (**e**, **f**). The surrounding noncancerous liver cells also showed expression of OATP1B8 (**b**), although the staining is weaker than that in the HCC cells in the peripheral region of the tumor (**d**)

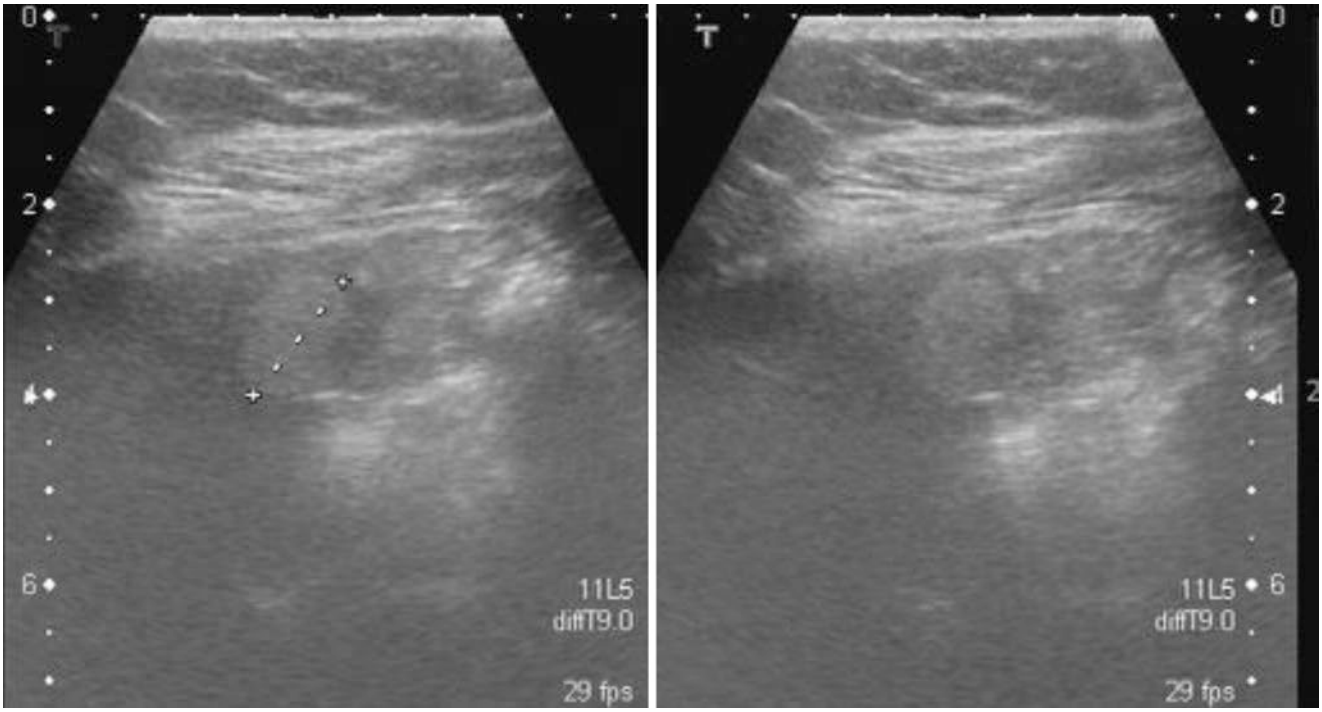

Fig. 17.3 US image of early HCC. The small high-echoic nodule (15 mm) is observed in the peripheral region of the right lobe

- Intermediate stage (B): multinodular tumors in the liver, PS 0, and Child-Pugh A or B.
- Advanced stage (C): HCC with vascular invasion and metastasis to lymph nodes or other body organs. PS 1 or 2. Child-Pugh A or B.
- Terminal stage (D): PS 3 or 4 or Child-Pugh C.

Based on this classification, patients with very-early- to early-stage HCC should be treated curatively, such as with resection, radiofrequency ablation (RFA), and liver transplantation. Transarterial chemoembolization (TACE) is recommended for intermediate-stage HCC cases. However, based on the recent advancement of molecular targeted therapies, intermediate stage of HCC could also be a target of molecular therapy if patients are refractory to TACE. Advanced-stage HCC is a candidate for molecular therapy, such as sorafenib, regorafenib, and lenvatinib [17–19]. HCC patients in terminal stage generally receive supportive care.

Case 17.2 (Early HCC)
An early HCC case in a patient with HCV-positive liver cirrhosis is presented herein. The patient underwent resection of a tumor emerging in the peripheral region of S6. B-mode US image represented a 1.5 cm highly echoic nodule (Fig. 17.3). Angio-CT showed a small low-density tumor before injecting contrast medium without significant enhancement in early and delayed phases, suggestive of a hypovascular tumor with fatty component (Fig. 17.4). The high-intensity tumor in in-phase T1-weighted image was depicted as low-intensity in out-of-phase image, indicating steatosis of the tumor. The tumor was hypovascular in the early-phase image of contract-enhanced MRI (Fig. 17.5). Macroscopically, tumor margin was unclear without fibrous capsule, and there were no findings of expansive growth. Diffuse fatty change and various numbers of portal tracts were observed within the tumor. Microscopically, increase of cell density, nuclear atypia, and stromal invasion are also observed (Fig. 17.6).

Case 17.3 (Progressed HCC)
A 44-year-old HBsAg-positive male, who underwent serological examinations a few times each year, was found to have an elevated alpha-fetoprotein (AFP) level of 56 ng/mL. Ultrasonography (US), computed tomography (CT), and angiography showed HCC with 1.5 cm in diameter in S8 (Fig. 17.7).

Case 17.4 (Hepatocellular Carcinoma)
A 64-year-old male with positive HCV RNA serum was referred for interferon therapy. His liver chemistry showed T-BIL 0.5 mg/dL, AST 49 IU/L, ALT 40 IU/L, ALP 301 IU/L, GGT 207 IU/L, hyarulonic acid 182 ng/mL, HCV genotype 1b, AFP 6.5 ng/mL, PIVKA-II 443 mAU/mL, PT 86%, PLT 17 × 10^4/μL, and $ICGR_{15}$ 12%. Abdominal US showed two neighboring space-occupying lesions in the S5 area. CEUS revealed large hypervascular and small hypovascular tumors in arterial phase. Defect of contrast medium was observed in both tumors in Kupffer phase (Fig. 17.8). CECT also showed large hypervascular and small hypovascular tumors in the early phase and defect on both tumors in the late phase; CT with angiography showed a hypervascular pattern in the larger

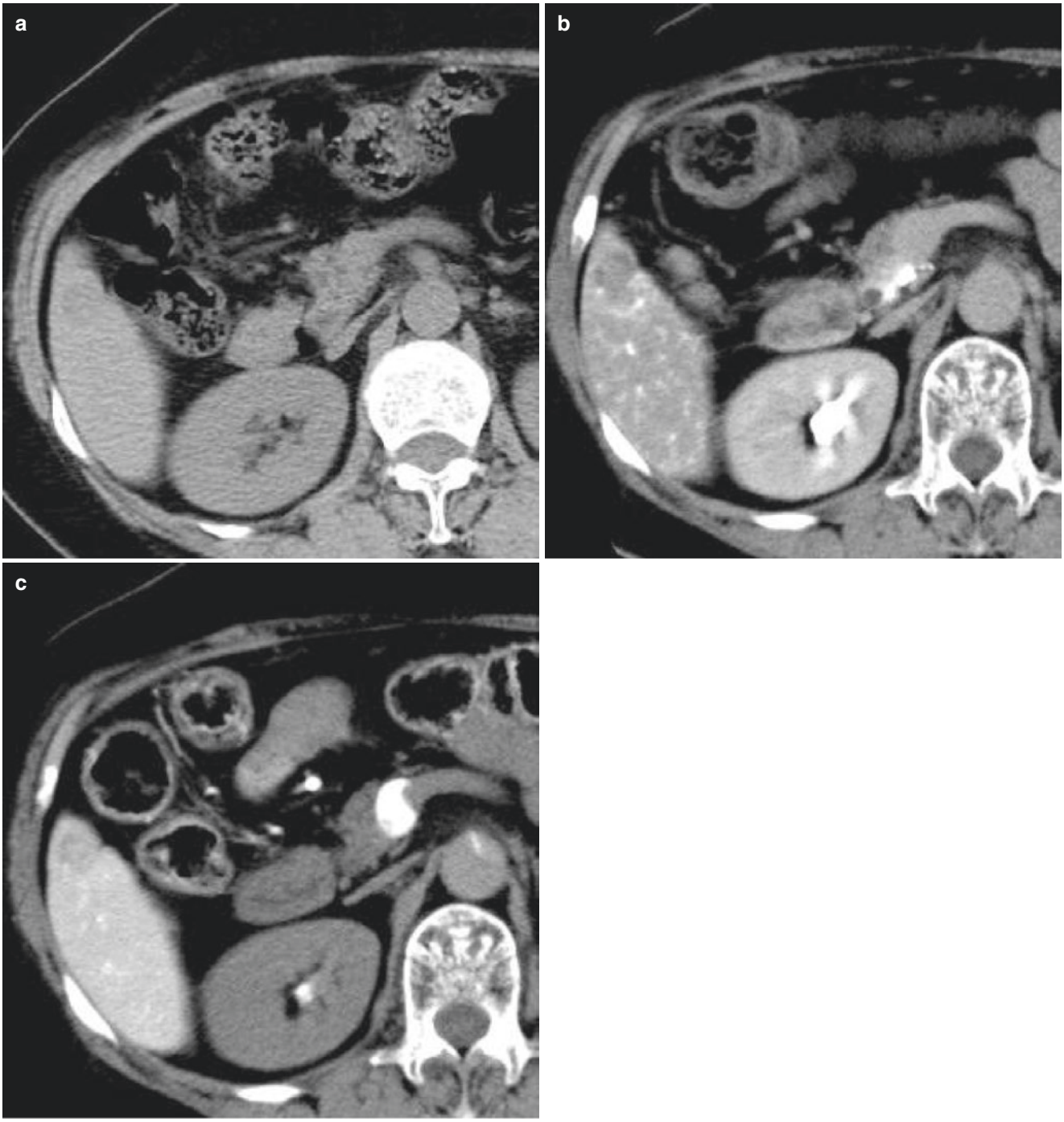

Fig. 17.4 Angio-CT for early HCC. The small low-density nodule is observed in S6 in plain CT image (**a**). CT arteriography (CTA) revealed the hypovascular tumor (**b**). CT arterial portography (CTAP) showed decrease of portal flow in the tumor (**c**)

tumor and a hypovascular pattern with partially enhanced area in the small tumors in the arterial phase; both tumors showed defect in the venous phase (Fig. 17.9). MRI showed low-intensity and high-intensity tumor in T1-weighted image and high intensity in both tumors in T2-weighted image; Gd-EOB-DTPA-enhanced MRI revealed enhancement in the former and defect in the latter in the vascular phase (Fig. 17.10). The resected large tumor was necrotic in the center. Both tumors were surrounded by capsules. Neoplastic cells formed trabecular and partially glandular structures with canalicular and intracytoplasmic bile (Fig. 17.11). In the small tumor, necrosis with viable neoplastic cells was observed within the surrounding fibrosis (Fig. 17.12).

The treatment for HCC is either surgical or nonsurgical. Surgical interventions include resection or transplantation. Nonsurgical procedures include TACE or hepatic arterial

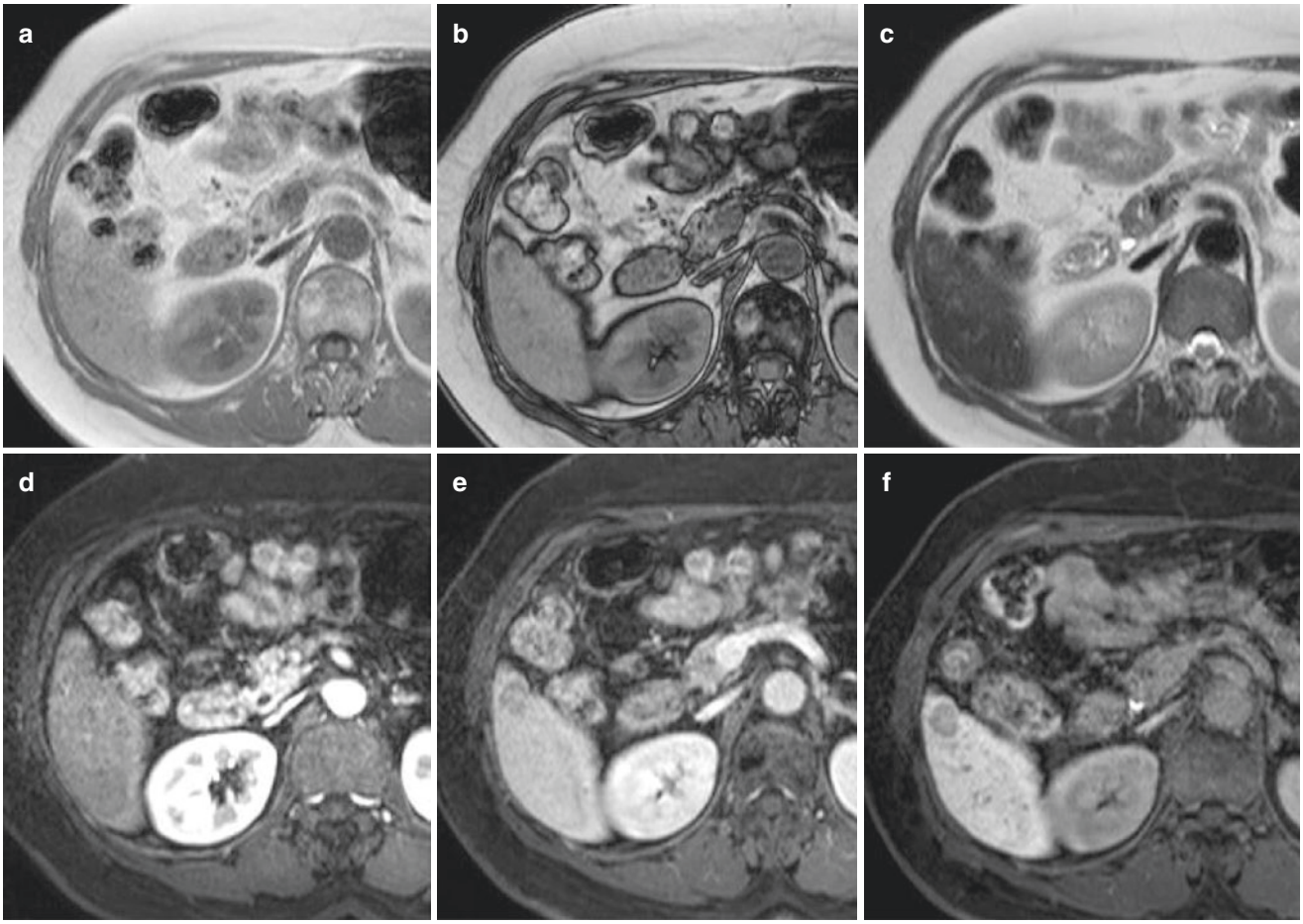

Fig. 17.5 MRI images of early HCC. In-phase T1-weighted image (**a**), out-of-phase T1-weighted image (**b**), T2-weighted image (**c**), arterial-phase image of Gd-EOB-DTPA contract-enhanced MRI (**d**), portal phase image of Gd-EOB-DTPA contract-enhanced MRI (**e**), and hepatobiliary phase image of Gd-EOB-DTPA contract-enhanced MRI for the tumor in S6. The high-intensity tumor in the in-phase T1-weighted image was depicted as low-intensity in out-of-phase image, suggesting the fatty change of the tumor. The tumor was revealed hypovascular in the contract-enhanced MRI images

infusion chemotherapy (HAIC), RFA [14], percutaneous ethanol injection (PEI) [20], or systemic therapy [21]. Figure 17.13 shows the HCC case treated with TACE. Resected tumor shows necrosis after embolization, and the internodular nonneoplastic liver parenchyma is hemorrhagic (Fig. 17.14).

The use of an anticancer drug doxorubicin or cisplatin with Lipiodol in HAIC resulted in specific retention in the tumor and induced complete necrosis surrounded by fibrous capsule (Fig. 17.15). Figure 17.16 shows the HCC case treated with PEI. US reveals the HCC with a halo; the lesion turned hyperechoic after PEI; and the resected tumor is encapsulated by a fibrous tissue with complete necrosis and hemorrhage (Fig. 17.16). Figure 17.17 shows the histology of HCC tissue after RFA with massive necrosis surrounded by fibrosis. After TACE, TAI, PEI, and RFA therapy, viable cells often remain inside or outside the fibrous capsule (Fig. 17.18). Sarcomatous change is sometimes observed in HCC after TACE or TAI treatment (Fig. 17.19).

Prognosis of HCC is dependent on its size, infiltrative growth, and metastatic spread, as well as the functional capacity of the non-tumorous part of the liver [14]. HCC may be complicated by arterioportal fistula formation, esophageal varices, and pulmonary hypertension with liver cirrhosis. In most cases, circulatory or renal failure occurs after retention of massive ascites, portal thrombosis of the tumor, and tumor rupture.

17.3 Intrahepatic Cholangiocarcinoma (Cholangiocellular Carcinoma)

Carcinoma of the biliary epithelium can arise anywhere in the intrahepatic or extrahepatic bile ducts. Tumors originating from the bile ducts are classified into three types according to the site. Depending on whether they arise in the liver, near the hilum, or from the extrahepatic ducts, they are called intrahepatic or peripheral cholangiocarci-

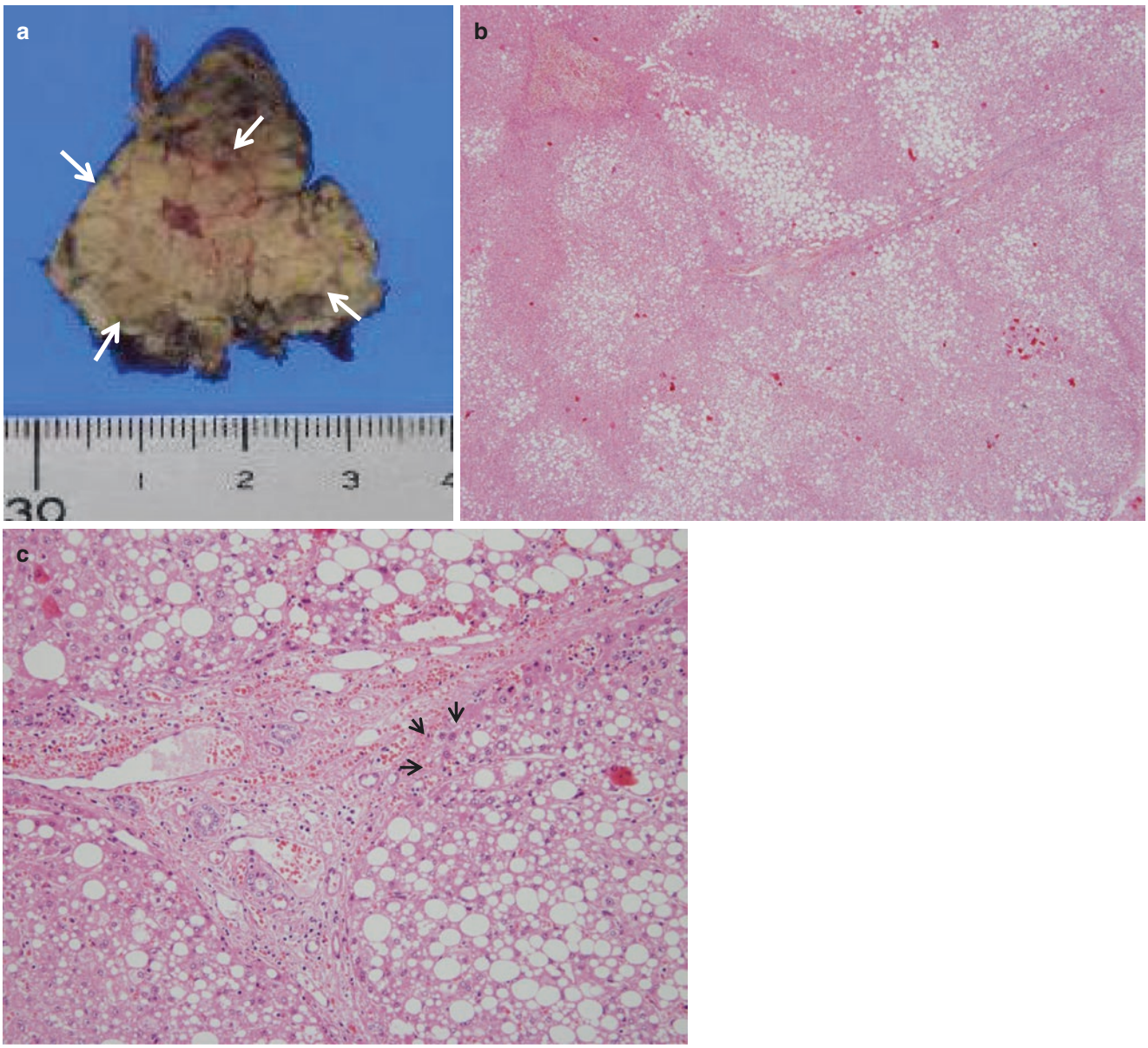

Fig. 17.6 Macroscopic and microscopic images of early HCC. Macroscopic view (**a**). Tumor with unclear margin and no fibrous capsule is observed (white arrow); tumor does not show an expansive growth pattern. Microscopic views (**b**, **c**). Diffuse fatty change and various numbers of portal tracts are observed within tumor. There is no fibrous capsule; tumor is distinguishable because of the steatosis (**b**: magnification, 40×). Increase of cell density and nuclear atypia are observed at magnification of 200× (**c**). Stromal invasion is observed (arrow)

noma, perihilar cholangiocarcinoma (including Klatskin tumor), and distal cholangiocarcinoma, respectively [22]. In addition, a subtype of CCC, morphologically similar to cholangioles, is known as cholangiolocellular carcinoma (CoCC), which is thought to arise in the canal of Hering (Fig. 17.20) [23]. It is reported that hepatic stem cells reside in the canal of Hering [24]. In addition, CoCC sometimes contains minor HCC components within the tumor, suggestive of hepatic stem cell origin. On the other hand, primary liver carcinomas with both hepatocytic and cholangiocytic differentiation have been referred to as "combined (or mixed) hepatocellular-cholangiocarcinoma" [25].

17.3.1 Etiology

Chronic inflammation of the bile duct could cause cholangiocarcinoma (CCC). The common predisposing factors are

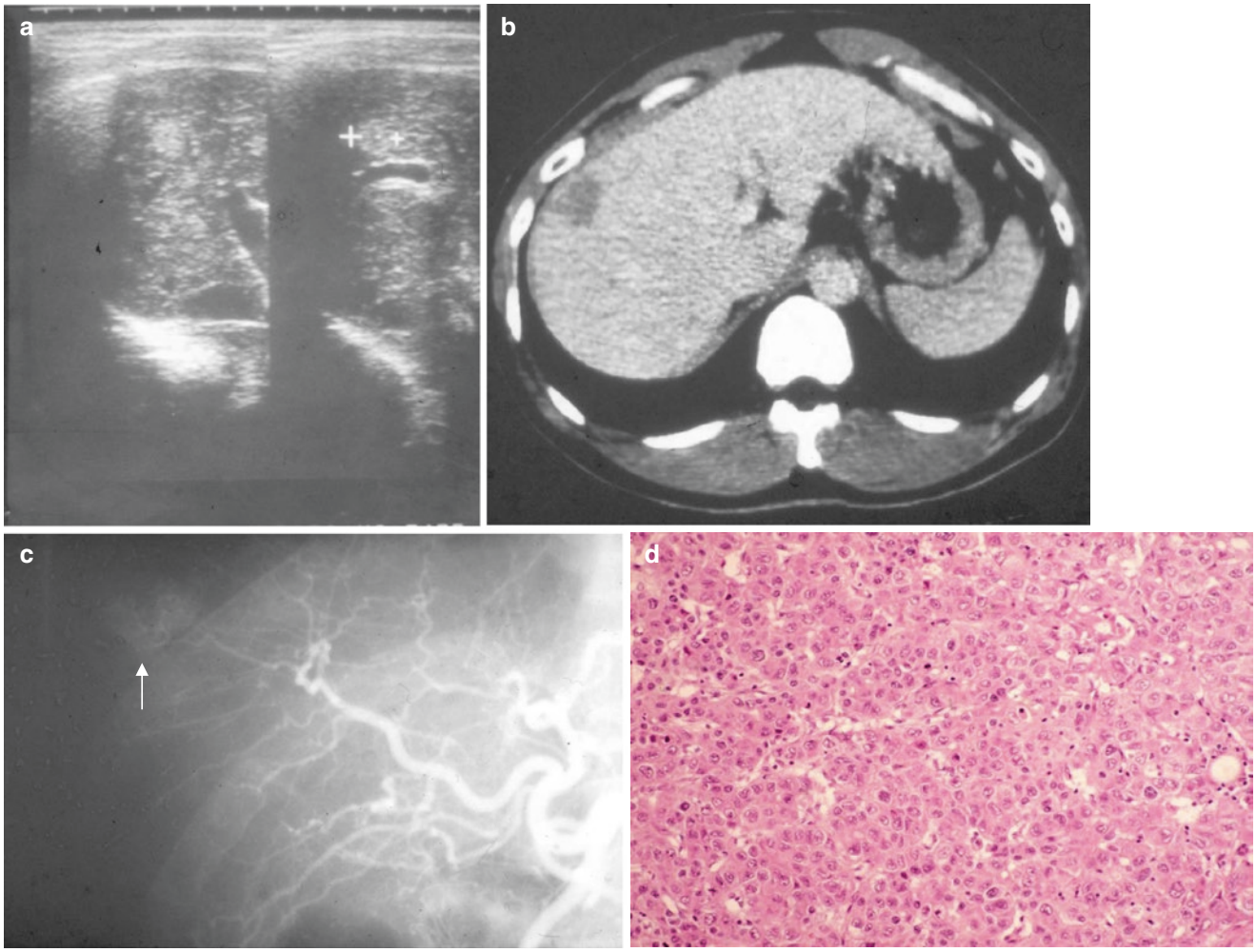

Fig. 17.7 Progressed hepatocellular carcinoma. US shows hyperechoic lesion of diameter 1.5 cm in S8 (**a**). CT with contrast medium shows the presence of a low-density area in the late phase (**b**). Common hepatic arteriography shows tumor staining (arrow) in S8 (**c**). The resected tumor tissue shows moderately differentiated type of hepatocellular carcinoma (**d**)

infestation with flukes [26], hepatolithiasis [27], primary sclerosing cholangitis, and congenital cystic diseases of the bile ducts [28]. Organic solvent, such as dichloromethane and 1,2-dichloropropane, and radioactive radiological contrast medium (Thorotrast) also induce CCC [29].

Interestingly, CCC is also divided into four subgroups based on the gene mutation and expression signature [30]. CCC caused by flukes infection is characterized by the hypermethylation on the promoter CpG, decrease of ten-eleven translocation methylcytosine dioxygenase 1 (TET1) expression, increase of histone methyltransferase enhancer of zeste homolog 2 (EZH2) expression, and frequent somatic mutation of AT-rich interactive domain-containing protein 1A (ARID1) gene, suggesting that epigenetic mechanism should be involved in carcinogenesis for this type of CCC. It is also reported the difference of mutation profile that should drive carcinogenesis among CCCs originated from different sites of bile tree [31]. These evidences suggested that difference of genetic and epigenetic alterations of CCC should be, at least partially, affected by its etiology. On the other hand, morphologically, the tumors are classified into mass-forming, periductal-infiltrating, and intraductal-growth types [32].

17.3.2 Diagnosis

Mass-forming CCC is a circumscribed tumor with lobular configuration and no capsule, while the periductal-infiltrating CCC is highly invasive and sometimes undetectable by US. Intraductal-growth CCC causes intraductal mass, obstruction, and dilatation of the bile duct. CEUS images of CCC generally show slightly hypervascular pattern. Ring enhancement of the tumor margin at early phase and delayed

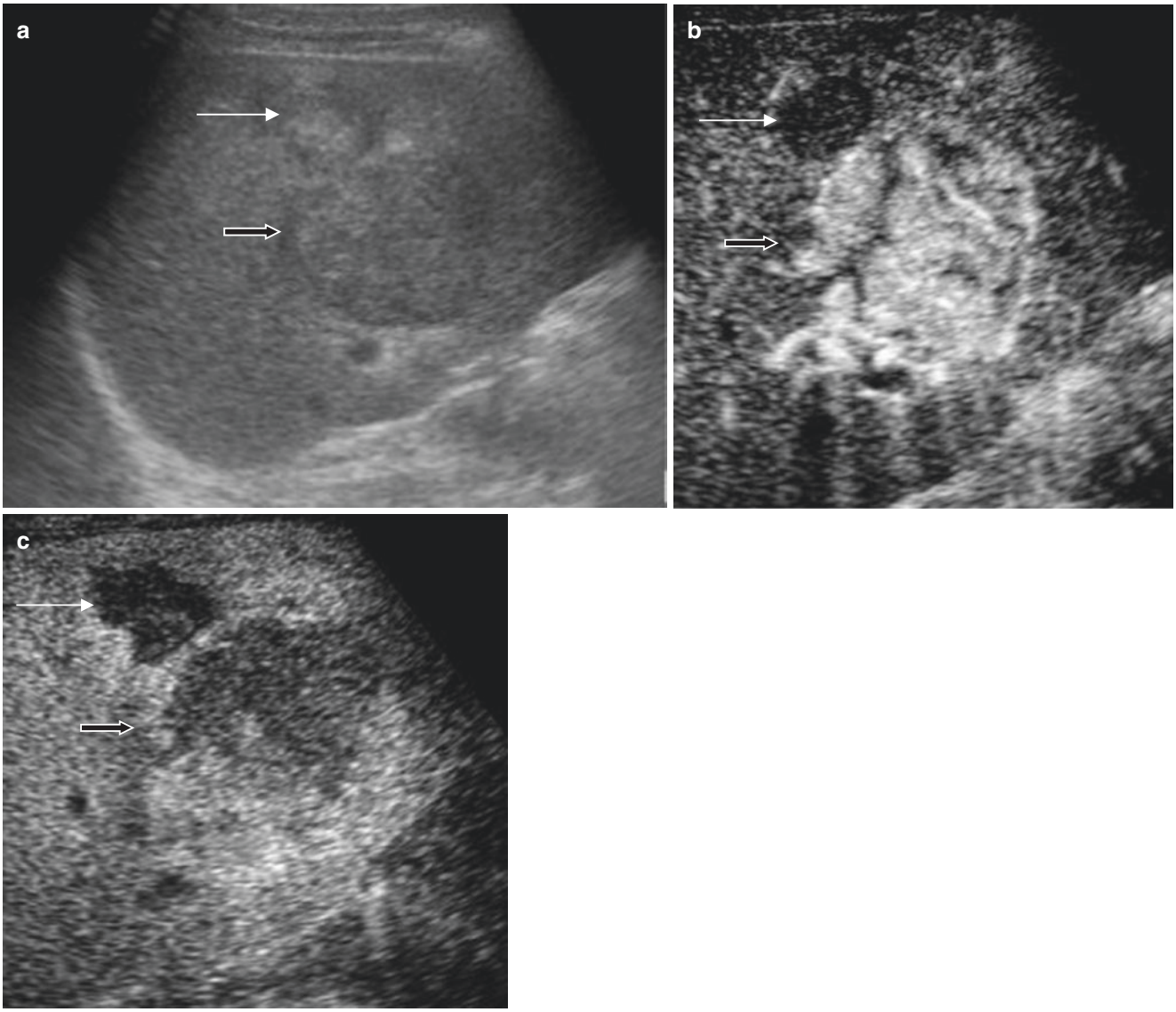

Fig. 17.8 Ultrasonographic findings with or without contrast medium in hepatocellular carcinoma. The isoechoic space-occupying lesion (SOL) (short arrow) with halo and a high-echoic SOL (long arrow) are mosaic in echo pattern (**a**). US image with contrast medium shows high echogenicity in the large SOL and low echogenicity in the small SOL in the vascular phase (**b**). A low-echoic pattern is seen in both SOLs in the Kupffer phase (**c**) (Courtesy of Dr. T. Mori)

enhancement can be detected in CCC cases, but these findings are also observed in metastatic tumors of the liver. MRI regularly shows low-intensity tumor on T1-weighted and high-intensity tumor on T2-weighted image [22].

17.3.3 Treatment

Surgical resection of tumor is the first line of the treatment; systemic chemotherapy using gemcitabine with/without cisplatin is generally the recommended treatment for unresectable cases. Radiation and chemotherapy are used for palliative treatment [33].

Case 17.5 (Cholangiocarcinoma, Mass-Forming Type)
A 66-year-old male presented with complaint of jaundice. US showed a large isoechoic tumor in S4 (Fig. 17.21). CT showed a tumor in S4 with delayed enhancement (Fig. 17.22). Percutaneous transhepatic cholangiogram showed dilatation of the right hepatic bile duct. US-guided tumor biopsy revealed glandular neoplastic structures with fibrosis (Fig. 17.23).

Case 17.6 (Cholangiocellular Carcinoma with Infection of *Clonorchis sinensis*)
A 72-year-old female presented with anorexia, general malaise, and jaundice. Her laboratory data showed T-BIL

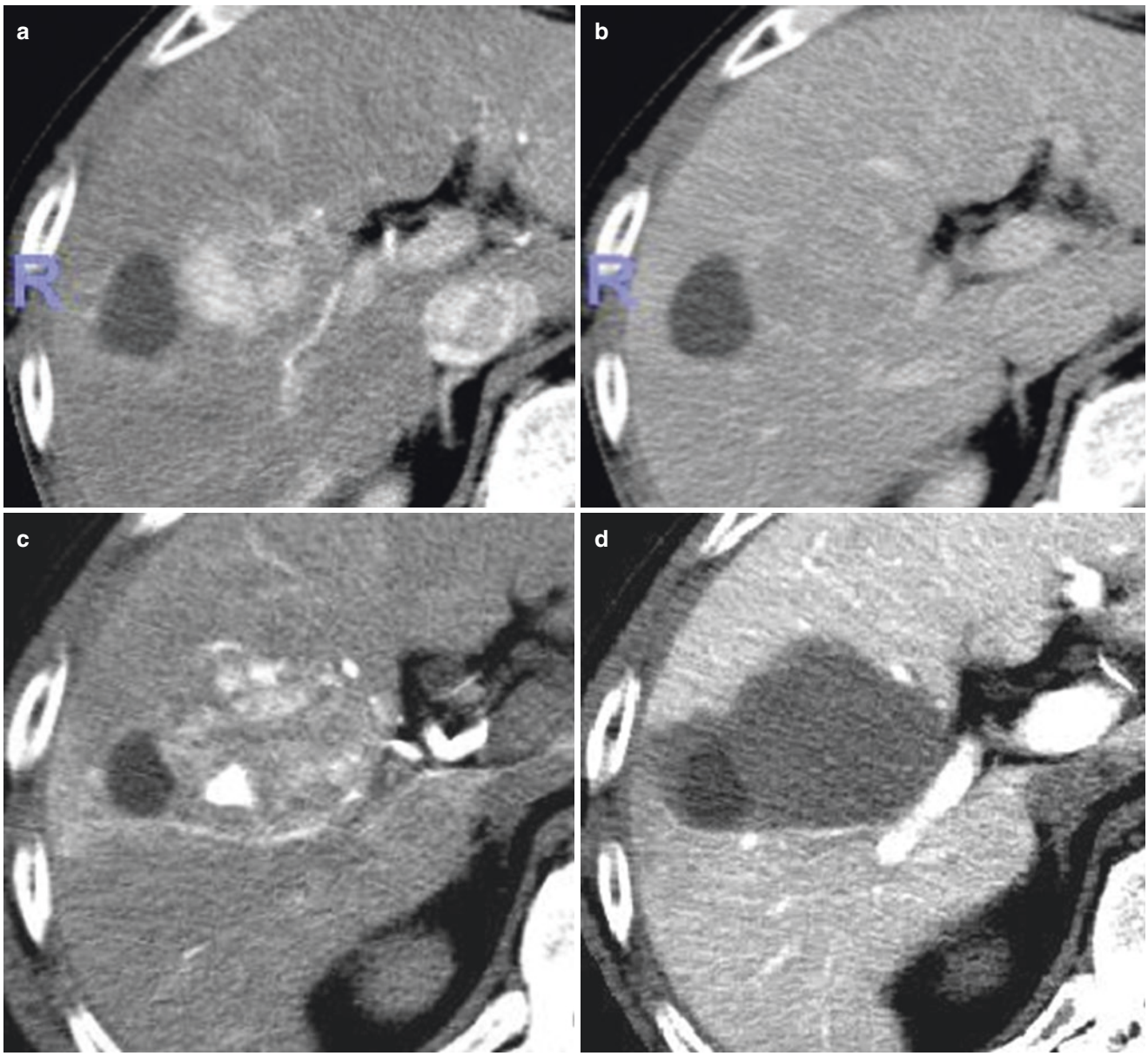

Fig. 17.9 CT with or without angiography in hepatocellular carcinoma. CECT shows high density in a large tumor and low density in a small tumor in the early phase (**a**), and iso- or low density is seen in both tumors in the late phase (**b**). Angio-CT revealed hypervascular in the former and in a partial area of the latter in the arterial phase (**c**). Angio-CT shows low density in both tumors in the venous phase (**d**) (Courtesy of Dr. T. Mori)

6.91 mg/dL, GOT 208 IU/L, GPT 315 IU/L, ALP 3952 IU/L, GGT 1194 IU/L, CRP 4.7 mg/dL, WBC 6400/mm^3, eosinophils 9.6%, and CA19-9 9788 IU/L. Endoscopic nasal bile d**rainage** and percutaneous transhepatic cholangiodrainage were performed when bilirubin reached 23.36 mg/dL. The bile juice contained *Clonorchis sinensis* eggs. Endoscopic retrograde cholangiopancreatography showed obstruction at the junction of the left and right biliary ducts and peripheral ductal dilatation. CECT revealed low-density area in the portal trunk, swelling of the para-aortic lymph nodes, and small multiple low-density areas in the liver. The patient died of liver failure. Autopsy showed dysplastic glands in the portal tract with fibrosis and infiltration of neutrophilic leukocytes. Cholangiocarcinoma is commonly associated with fibrosis (Fig. 17.24).

Case 17.7 (Cholangiocarcinoma with a Component of Cholangiolocellular Carcinoma)

A 75-year-old female presented with liver cirrhosis type C and a liver nodule. Laboratory tests revealed HBsAg negative, positive for HCV Ab, AST = 58 IU/L, ALT = 33 IU/L,

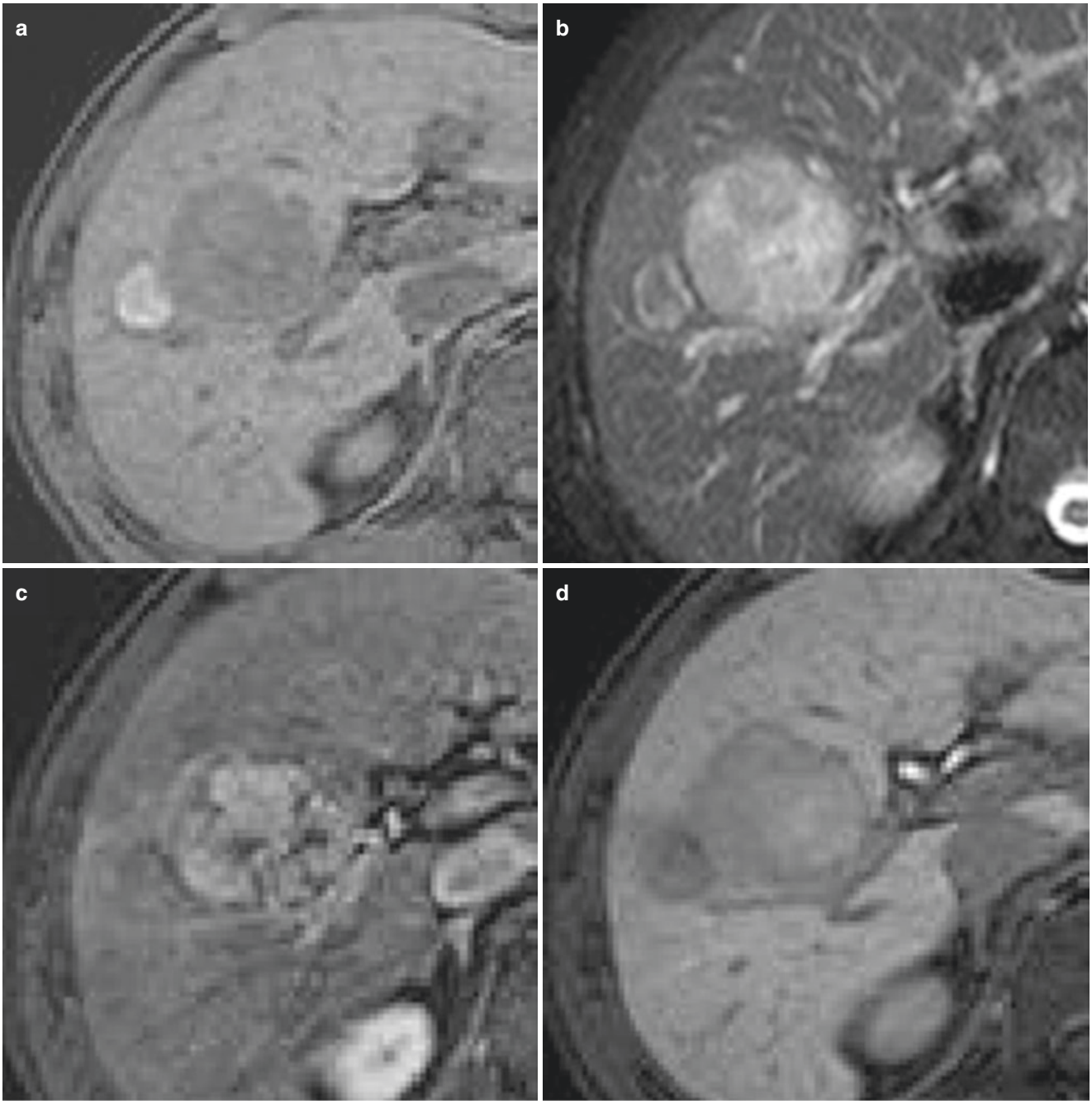

Fig. 17.10 Magnetic resonance image with Gd-EOB-DTPA in hepatocellular carcinoma. MRI with T1 intensification shows low density in a large tumor and high intensity in a small tumor (**a**). MRI with T2 intensification shows high intensity in the former and mixed intensity in the latter (**b**). Gd-EOB-DTPA-enhanced MRI image shows high intensity in a large tumor and iso-intensity in a small tumor in arterial phase (**c**); MRI with EOB shows low intensity in both tumors in hepatobiliary phase (**d**) (Courtesy of Dr. T. Mori)

ALP = 223 IU/L, AFP = 9.9 ng/mL, PIVKA-II = 25 mAU/mL, CEA = 3.7 ng/mL, and CA19-9 = 45.1 U/mL.

The B-mode image of US showed a low-echoic nodule in S4/8 (Fig. 17.25). The nodule showed slightly low density on plain CT, enhancement in the arterial phase, and partial defect in the central area (Fig. 17.26). The tumor revealed as defect in the hepatobiliary phase of the Gd-EOB-DTPA-enhanced image (Fig. 17.27). The tumor showed irregular margin and no capsule. Microscopic examination revealed the tumor consisted of CCC, CoCC, and poorly differentiated CCC components (Figs. 17.28 and 17.29).

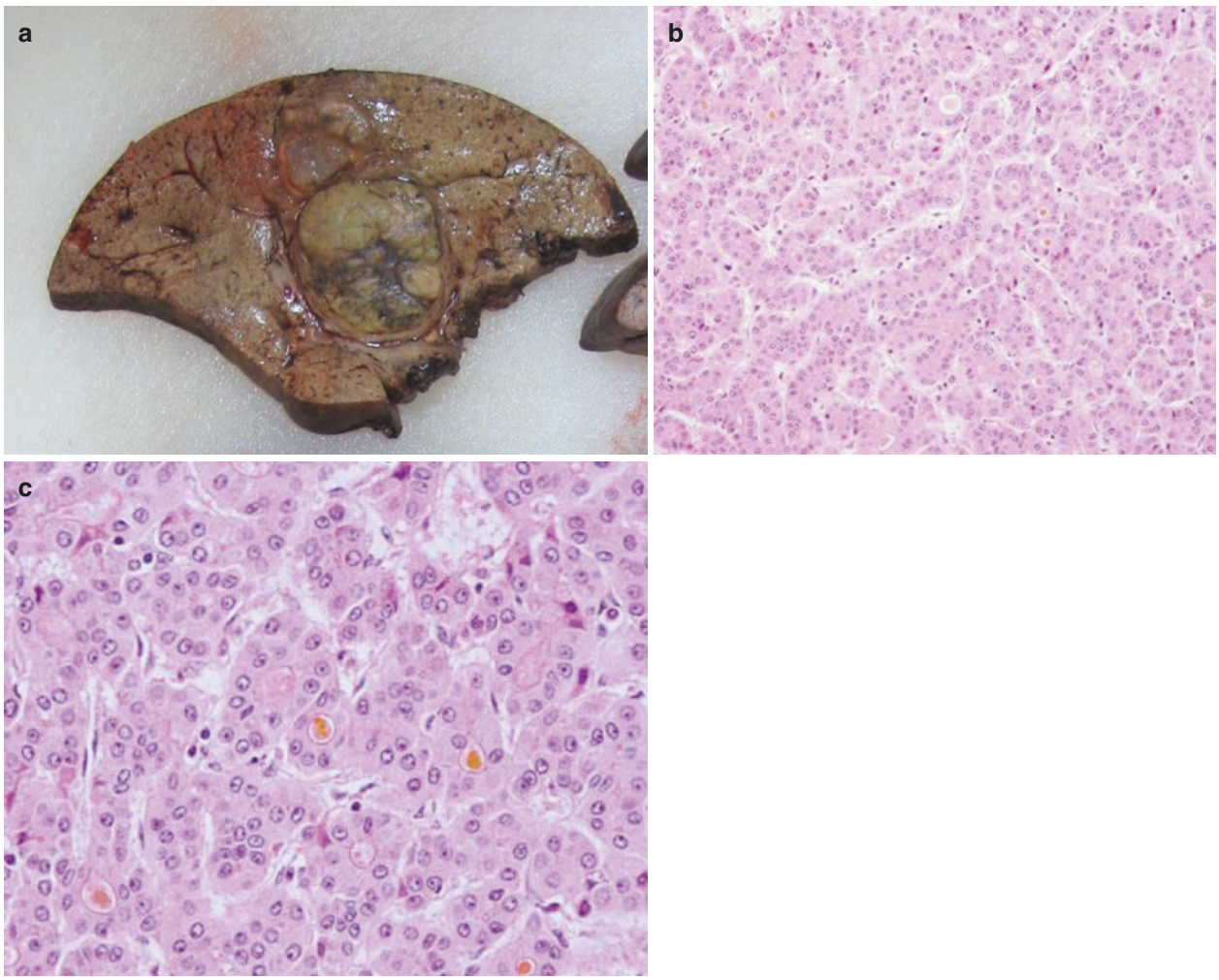

Fig. 17.11 Macro- or microscopic findings of hepatocellular carcinoma. Macroscopic findings of resected liver show a nodular tumor with a daughter nodule, and a necrotic area is seen in a main tumor (**a**). The main tumor shows trabecular type of hepatocellular carcinoma and a pseudoglandular structure is seen (**b**). Bile thrombus or cholestasis is seen in bile canaliculi and neoplastic cells (**c**) (Courtesy of Dr. T. Mori)

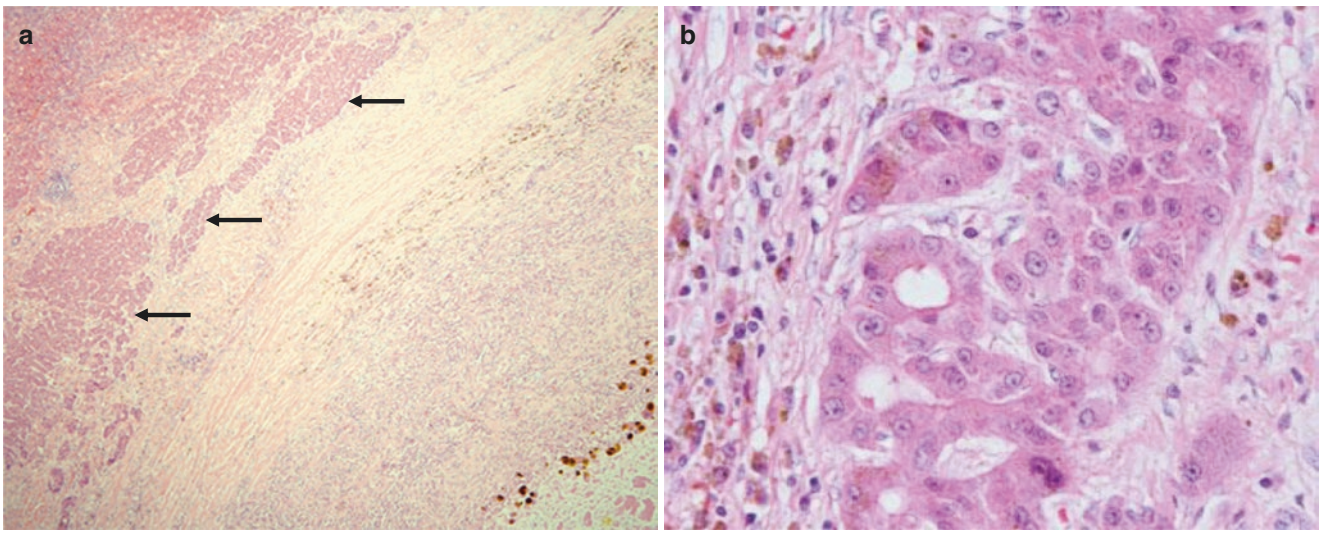

Fig. 17.12 Histological findings of hepatocellular carcinoma. A small tumor shows central necrosis with the presence of isolated tumor cells (arrow) in surrounding fibrosis (**a**). Neoplastic cells form trabecular and pseudoglandular structures (**b**) (Courtesy of Dr. T. Mori)

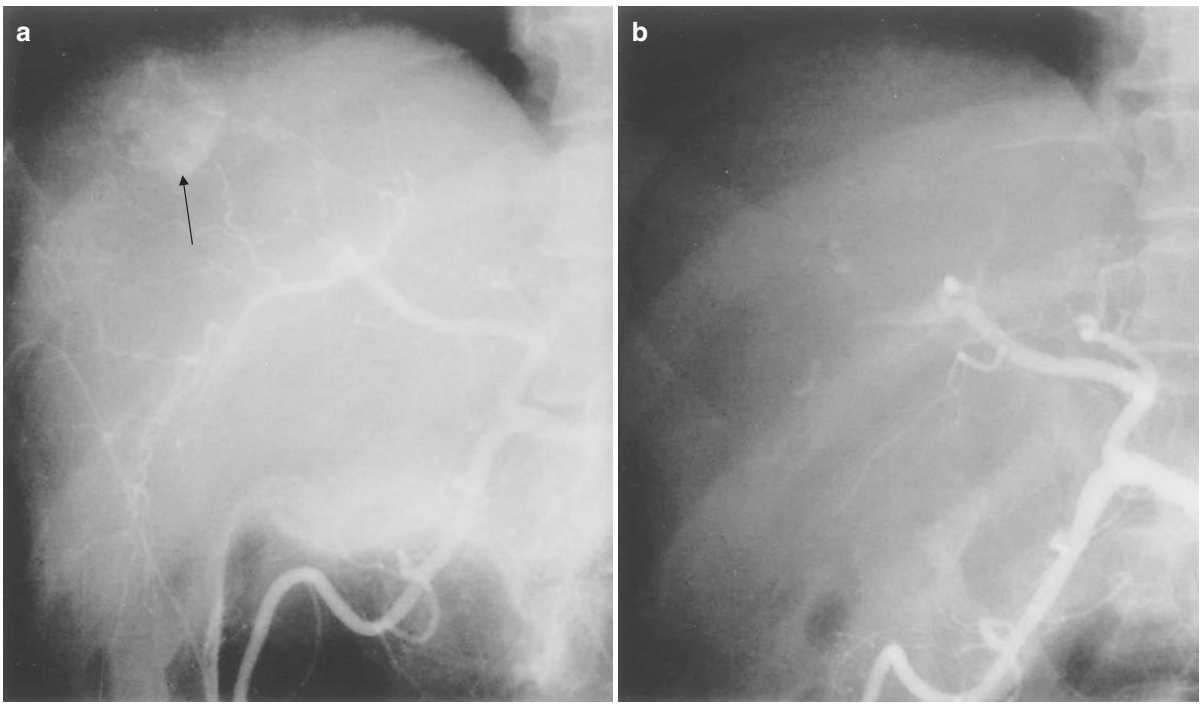

Fig. 17.13 Transarterial chemoembolization. The right hepatic angiography shows a hypervascular area (arrow) in S8 (anterosuperior subsegment of the right lobe) (**a**). Arteriography after TAE shows disappearance of arterial blood flow (**b**)

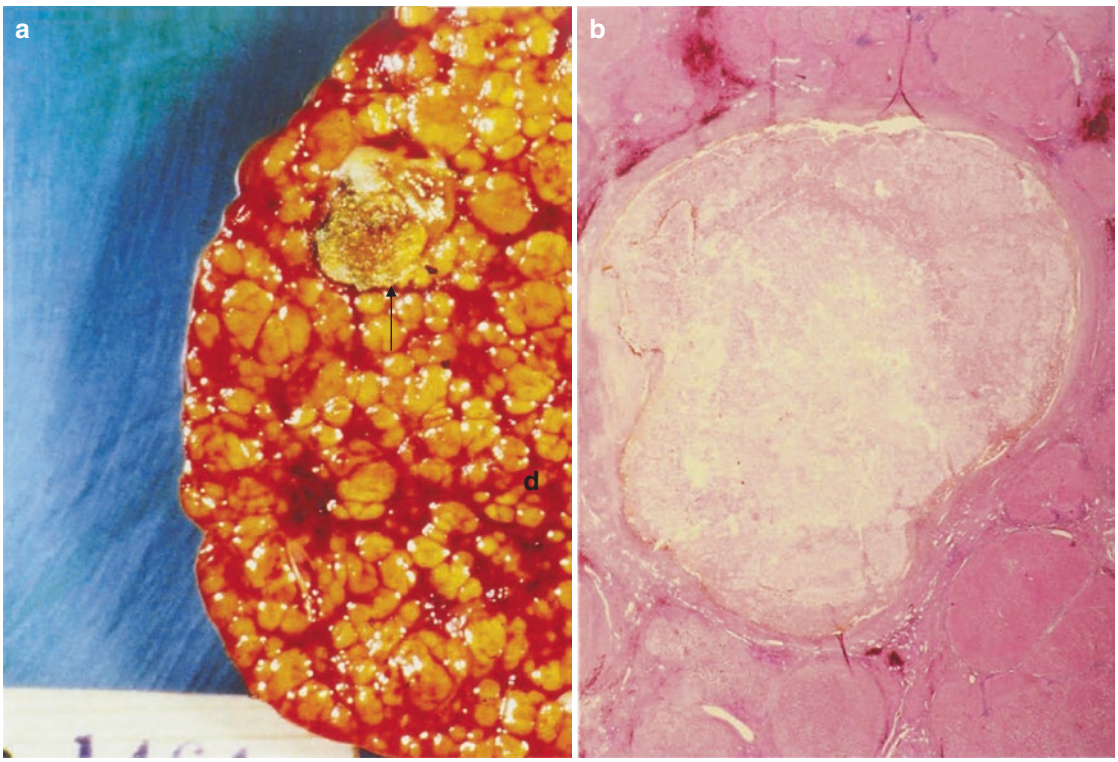

Fig. 17.14 Macro- and microscopic findings of the liver with hepatocellular carcinoma after transarterial embolization. Cut surface of the resected liver. The necrotic nodule (arrow) is surrounded by nonneoplastic regenerative nodules (**a**). Histology reveals an encapsulated tumor resulting in total necrosis. There is focal hemorrhage in the fibrous septa around the tumor (**b**)

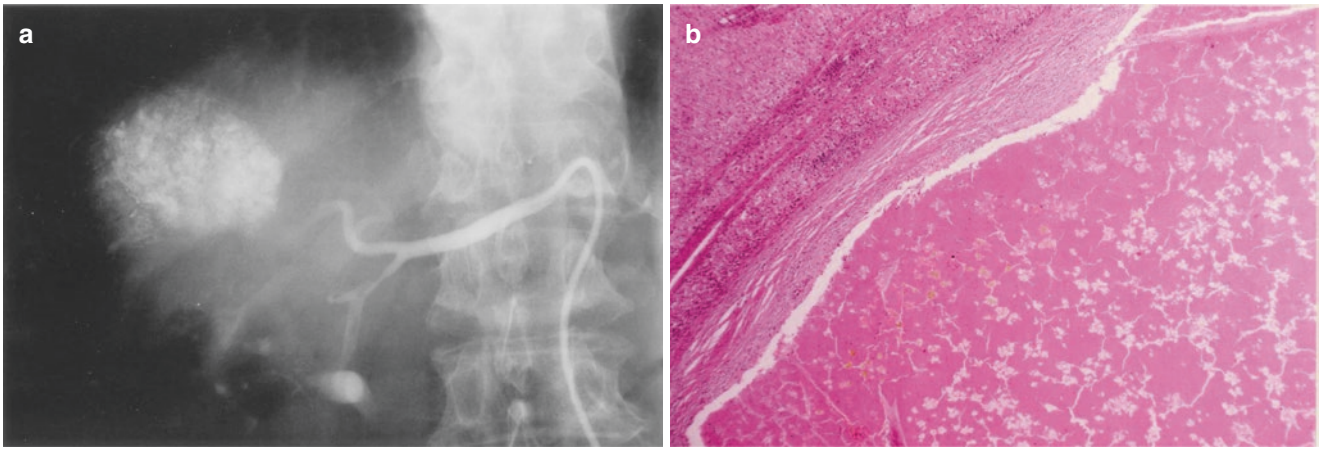

Fig. 17.15 Hepatic arterial infusion chemotherapy. Lipiodol is stained in the tumor area after infusion (**a**). The microscopic appearance confirms the complete necrosis of the tumor cells after hepatic arterial infusion chemotherapy (**b**)

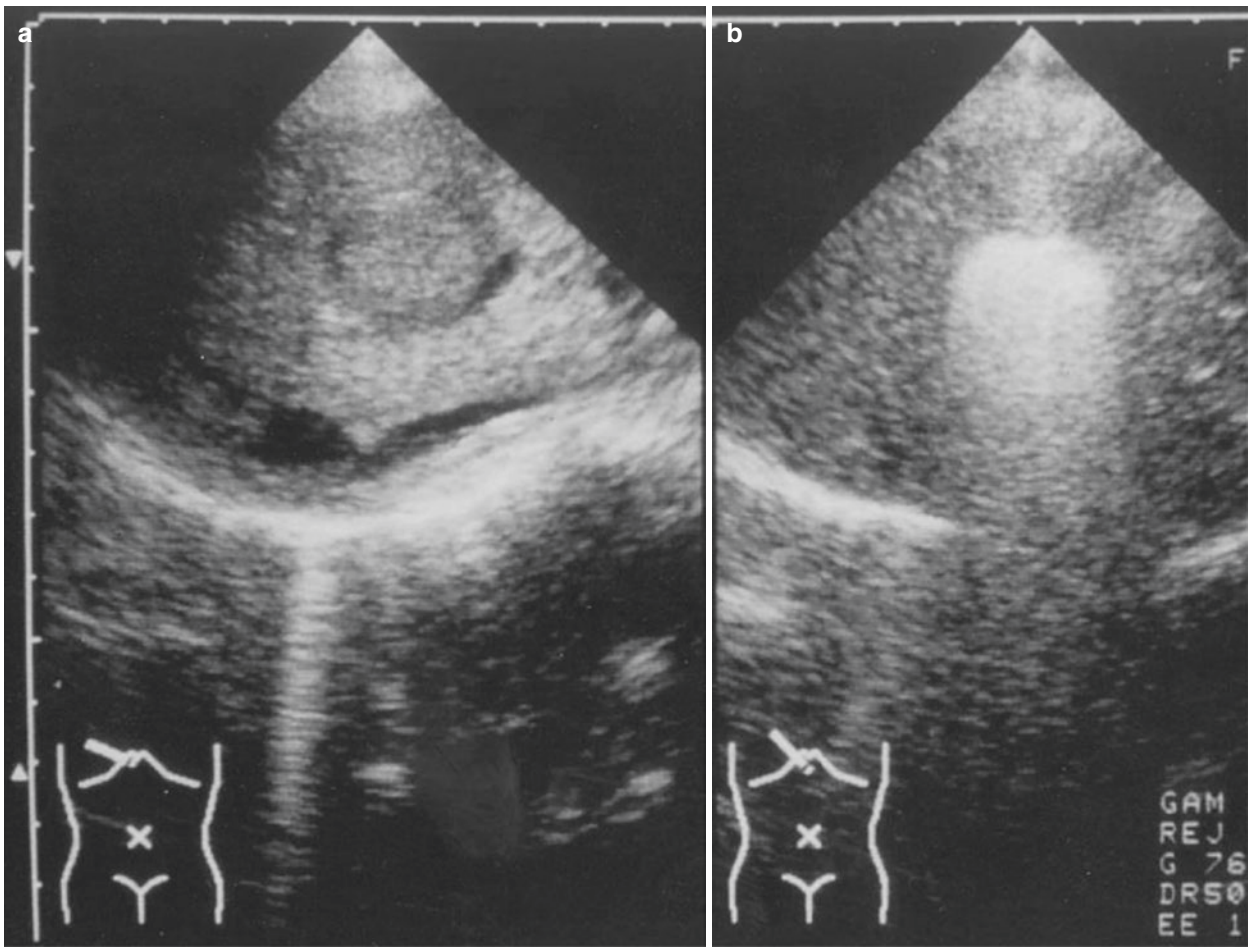

Fig. 17.16 Percutaneous ethanol injection. Ultrasonography shows an isoechoic space-occupying lesion (SOL) with halo (**a**). Ultrasonography shows hyperechoic SOL after PEI (**b**). The tumor (upper right) is totally necrotic. Nonneoplastic viable hepatocytes (lower left) are separated by fibrous connective tissue (**c**). The figures of this case are courtesy of Dr. Maki Iwai, Kyoto Prefectural University of Medicine

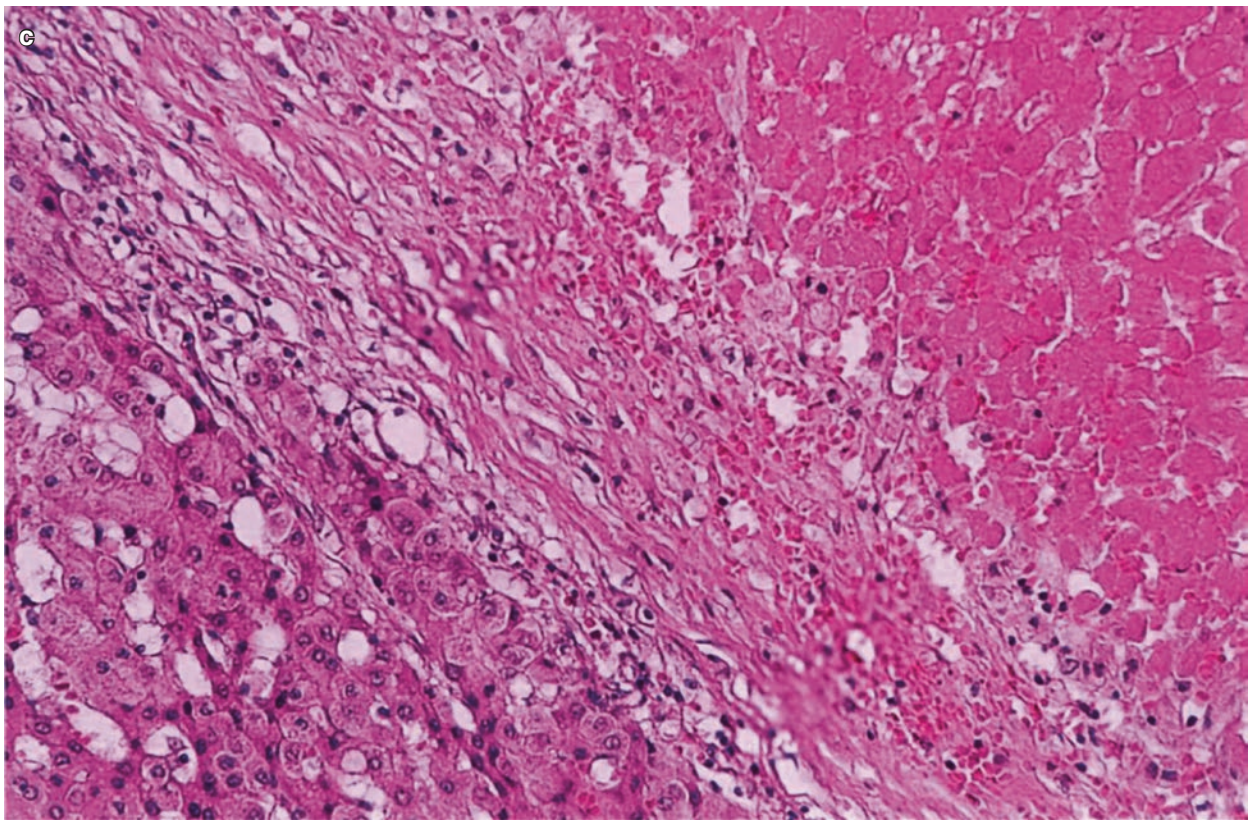

Fig. 17.16 (continued)

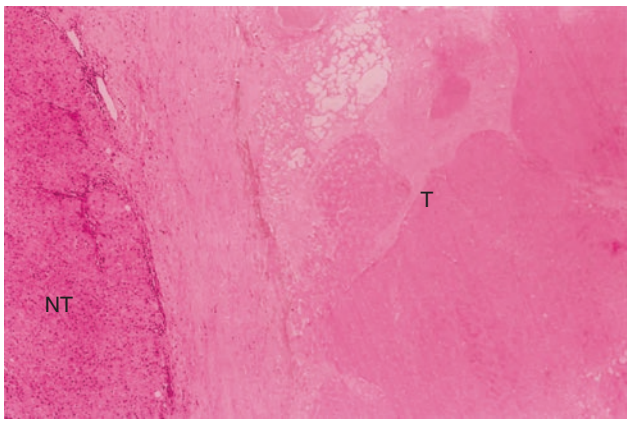

Fig. 17.17 Radiofrequency ablation. Massive necrosis of the encapsulated tumor (T) due to radiofrequency ablation NT, non-tumor

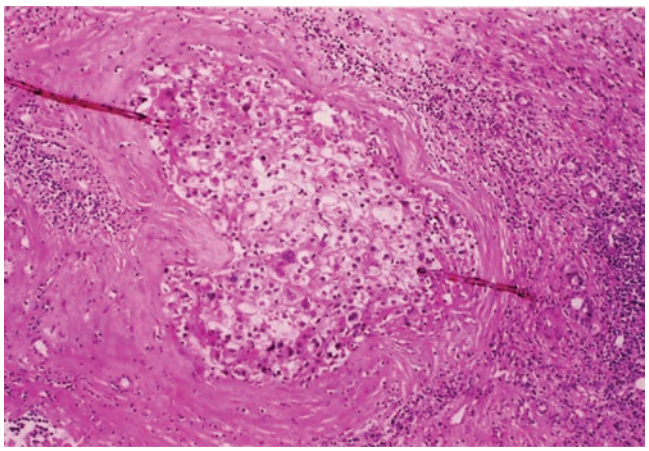

Fig. 17.18 Viable HCC cells after TACE. A small focus of viable neoplastic cells is remained in the fibrous capsule after TACE

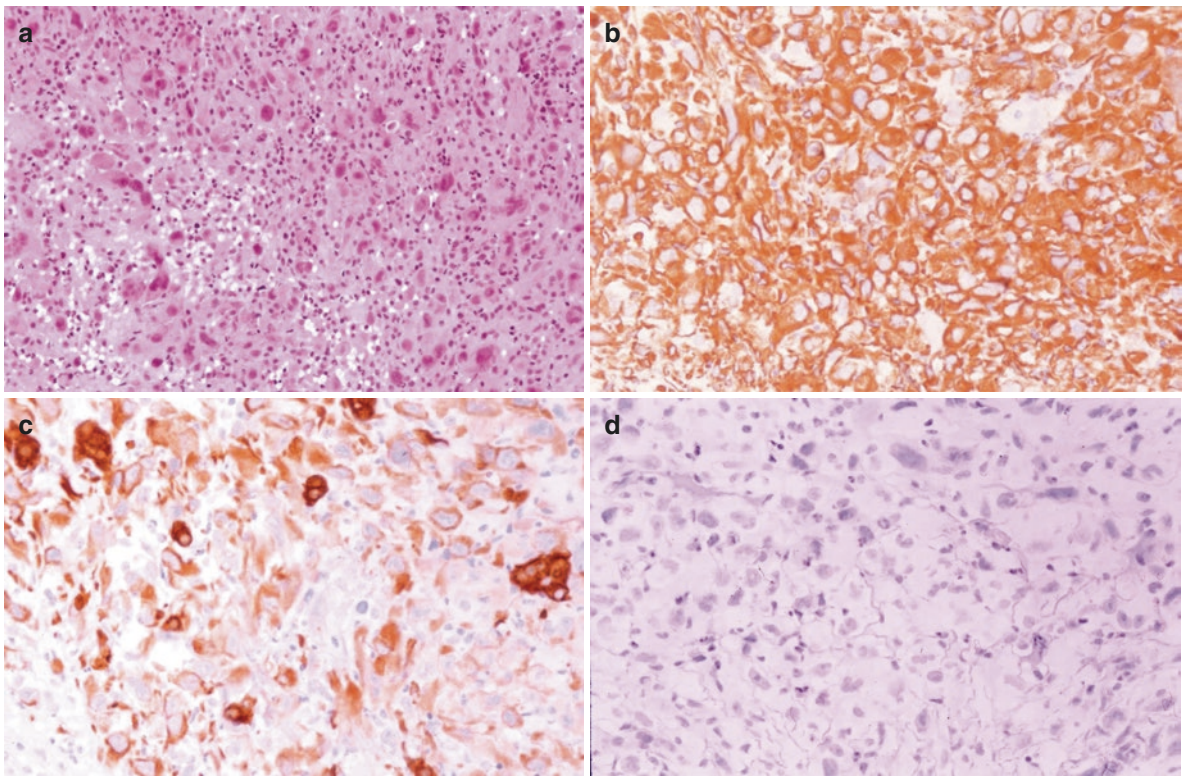

Fig. 17.19 Sarcomatous change in hepatocellular carcinoma. Multinucleated neoplastic cells are distributed with fibrous stroma cells (**a**). Expression of vimentin in neoplastic cells by immunohistochemistry (**b**). Cytokeratin (CK) 19 is stained in neoplastic cells (**c**). CK20 immunoreactivity is not detected in neoplastic cells (**d**)

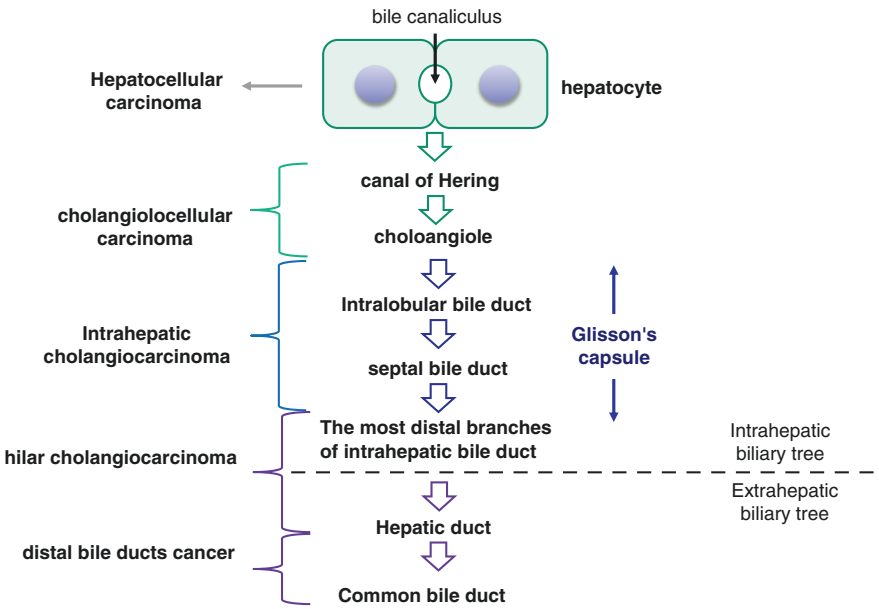

Fig. 17.20 Biliary tree and origin of cancer cell. Depending on whether they arise in the liver, near the hilum, or from the extrahepatic ducts, they are called carcinoma of the intrahepatic or peripheral bile duct, hilar cholangiocarcinoma (Klatskin tumor), or distal bile duct cancer, respectively. A subtype of CCC, morphologically similar to cholangioles, is known as cholangiolocellular carcinoma (CoCC), which is thought to be derived from Hering's canal. It is reported that Hering's canal might be composed of hepatic stem cells; CoCC sometimes contains HCC or CCC components within the tumor, suggesting that it could originate from hepatic stem cells

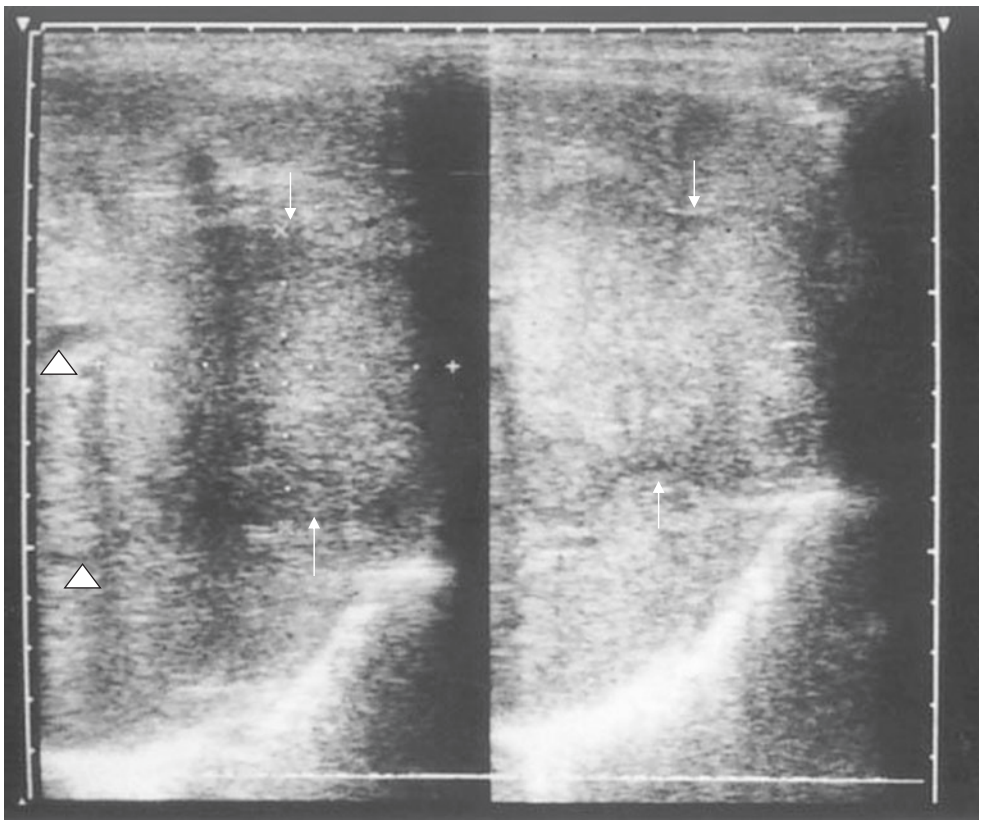

Fig. 17.21 Cholangiocellular carcinoma; US images. US shows an isoechoic tumor (arrow) in S4 and peripheral bile ducts (arrow head) are dilated around the tumor. The figures of this case are courtesy of Dr. Maki Iwai, Kyoto Prefectural University of Medicine

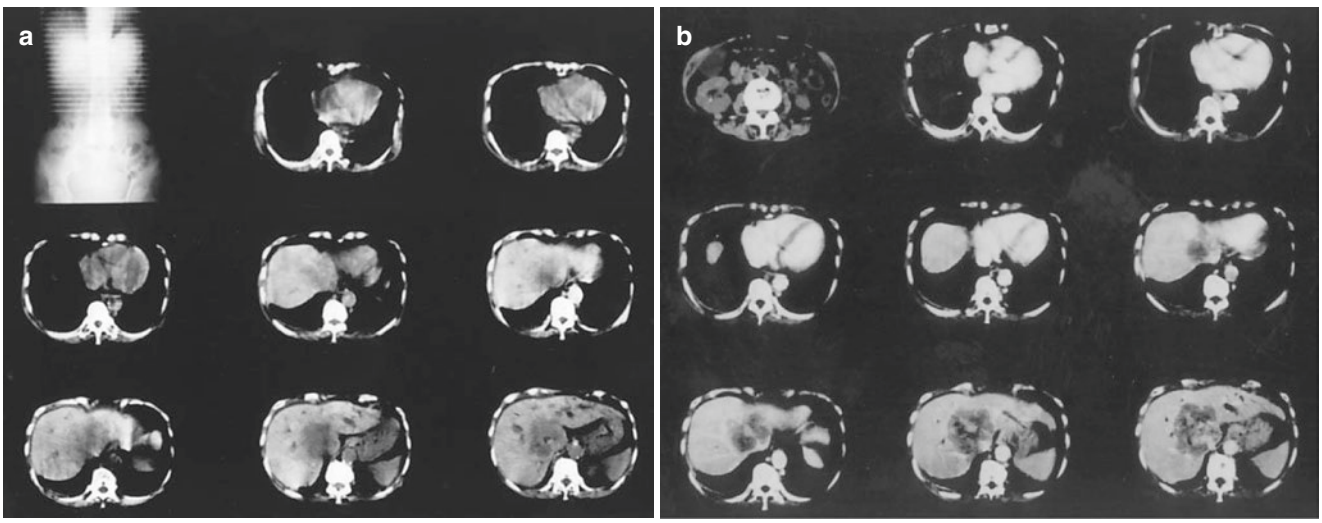

Fig. 17.22 Cholangiocellular carcinoma; CT images. CT shows a low-density area in S4 (**a**). A low-density area is partly enhanced by contrast medium (delayed enhancement); there is dilatation of the left intrahepatic bile duct and tumor invasion into the inferior vena cava (**b**)

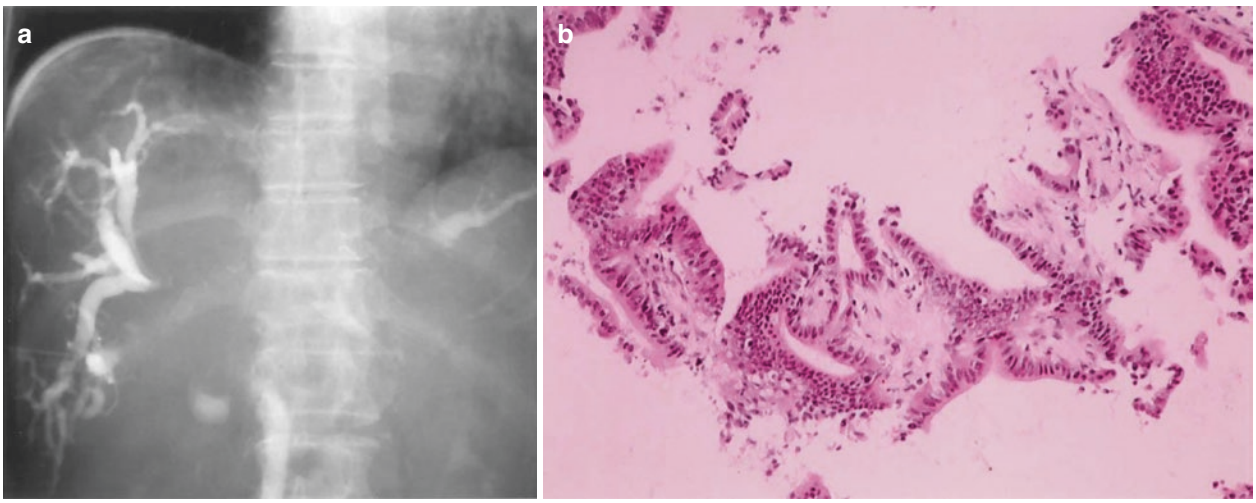

Fig. 17.23 Cholangiocellular carcinoma. Percutaneous transhepatic cholangiography (PTC) shows dilatation of the right and left intrahepatic bile ducts, and interruption of contrast medium is seen between the common and intrahepatic bile ducts (**a**). Needle biopsy of the tumor revealing neoplastic glands with focal loss of nuclear polarity and fibrous stroma (**b**)

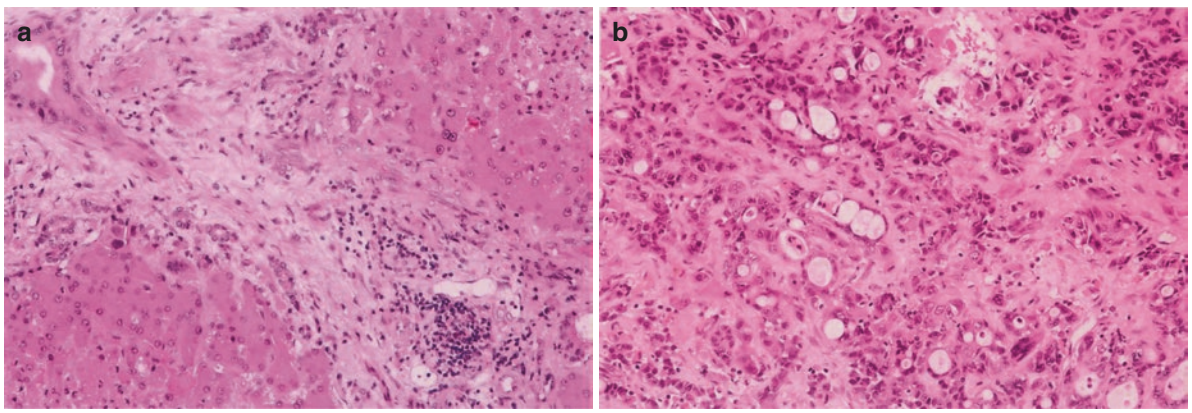

Fig. 17.24 Cholangiocellular carcinoma in the liver with infestation of *Clonorchis sinensis*. A neoplastic duct (upper left) is seen in the fibrous portal area with polymorphonuclear leukocyte infiltration, simulating a nonneoplastic interlobular bile duct (**a**). Poorly formed glands and cord-like structures are seen in the fibrous stroma (**b**)

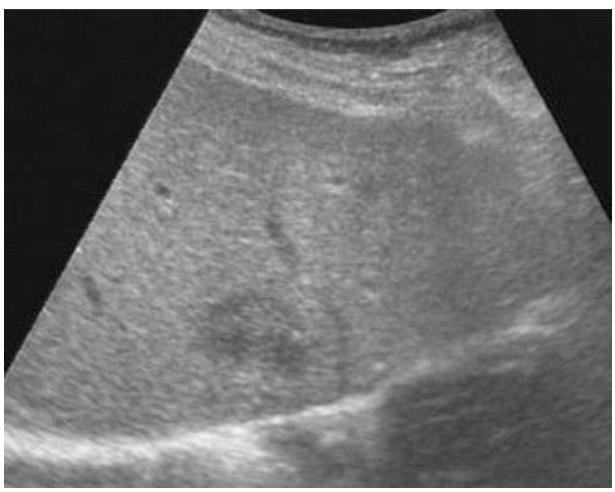

Fig. 17.25 Cholangiocellular carcinoma with the component of cholangiolocellular carcinoma; US images. The US showed a low-echoic nodule with heterogeneous isoechoic lesion inside

17.4 Mucinous Cystadenocarcinoma

Mucinous cystadenoma is regarded as a precursor or benign counterpart of mucinous cystadenocarcinoma [32]; the large majority occurs in middle-aged women and causes no symptoms or signs until the tumors are large. Metastasis is rare, and the tumor is considered as low-grade malignancy or carcinoma in situ when the neoplastic epithelium is contained within the cystic lesion. The operative results are good [34].

Case 17.8 (Mucinous Cystadenocarcinoma)
A 66-year-old male presented with an epigastric tumor, a high-echoic and papillary tumor with arterial flow (Fig. 17.30). CECT in the arterial phase revealed a low-density area with rim enhancement. In the delayed-phase image, the tumor is heterogeneous in density with prominent

Fig. 17.26 Cholangiocellular carcinoma with the component of cholangiolocellular carcinoma; CT images of the tumor. Plain CT image (**a**), arterial-phase image (**b**), portal-venous-phase image (**c**), and equilibrium-phase image (**d**) are shown. The nodule showed slightly low density in the pre-contrast, high density in the arterial, and partially low density in the central, accompanied with delayed enhancement in the peripheral region, in the portal-venous and equilibrium-phase image

rim enhancement pattern (Fig. 17.31). The T1-intensified image of MRI showed a mixture intensity in the tumor, and T2 image showed high intensity (Fig. 17.32). Angiography showed neovascularization and compression of the left hepatic artery. The resected tumor showed cystic structures surrounded by fibrous tissue and a cystic cavity lined by monolayer columnar epithelium. Much of the epithelium was desquamated. The remaining epithelium was basophilic and irregular in size, with displaced nuclei in the periphery. CA19-9 and carcinoembryonic antigen immunoreaction were seen in the cytoplasm, which contained mucinous material (Fig. 17.33).

Diagnosis of cystadenocarcinoma is made by both image analysis [35] and histological findings [32]. Resection leads to a high 5-year survival rate and good prognosis [36].

17.5 Hepatoblastoma

Hepatoblastoma is the most common liver tumor in childhood and is associated with congenital anomalies. The vast majority of cases are seen in children <5 years old, of which two-thirds are <2 years old. Boys are affected twice as frequently as girls. However, a few cases have been reported in middle-aged or

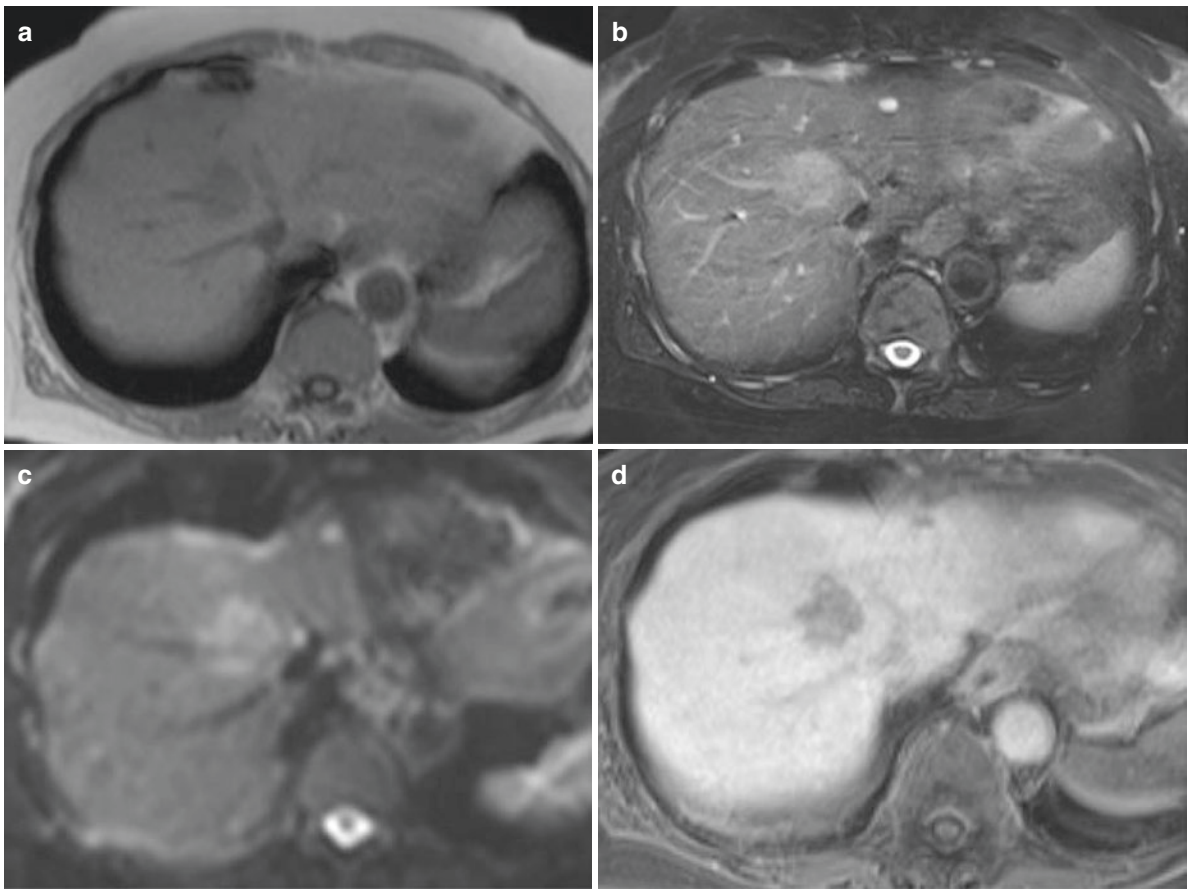

Fig. 17.27 Cholangiocellular carcinoma with the component of cholangiolocellular carcinoma; abdominal MRI images. The tumor revealed low intensity in the T1-weighted image (**a**) and high intensity in the T2-weighted and diffusion images (**b**, **c**). It was depicted as low-intensity nodule with irregular shape in the hepatobiliary phase of the Gd-EOB-DTPA-enhanced image (**d**)

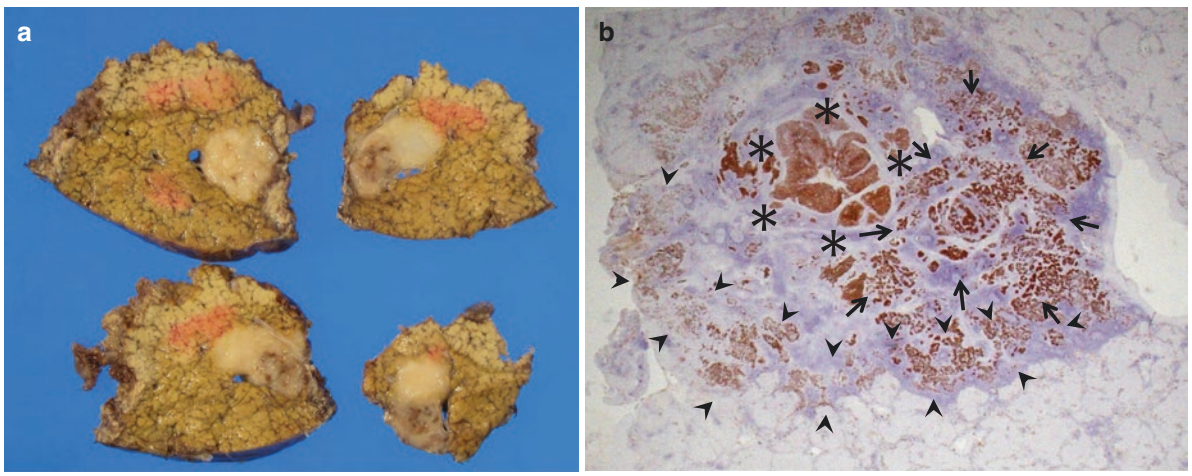

Fig. 17.28 Cholangiocellular carcinoma with the component of cholangiolocellular carcinoma; macroscopic view and loupe images. Macroscopic and loupe images of the tumor with CK7 immunostaining. Cross sections of the resected specimen (**a**). The tumor was whitish with an irregular boundary and without a capsule. Macroscopic view of the whole tumor with CK7 immunohistochemical staining (**b**). The tumor consisted of cholangiocellular carcinoma (CCC) components (arrow), cholangiolocellular carcinoma (CoCC) components (arrow head), and poorly differentiated CCC portion (asterisk)

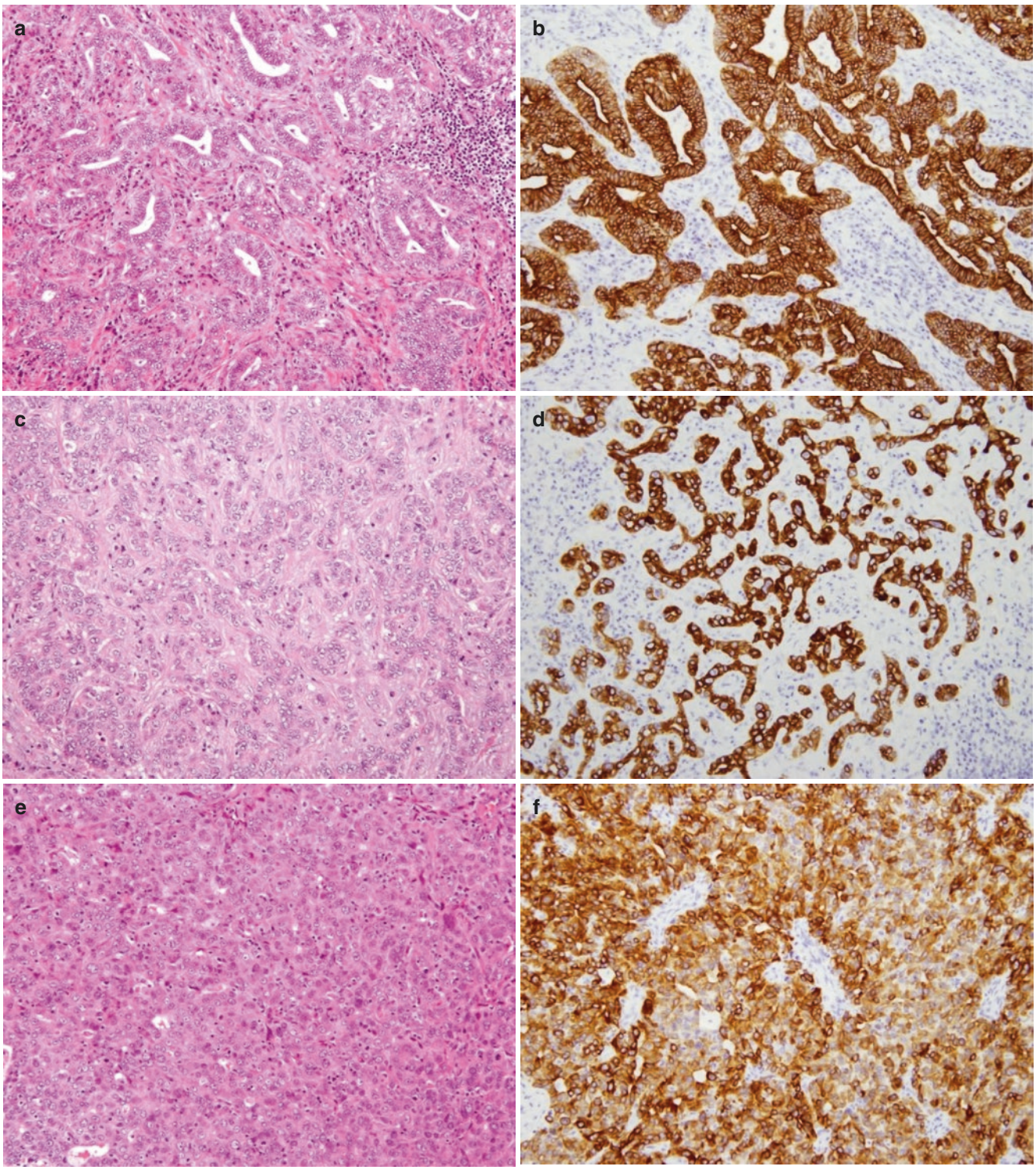

Fig. 17.29 Cholangiocellular carcinoma with the component of cholangiolocellular carcinoma; histologies and expression of CK7. Microscopic images of the tumor with HE and CK7 immunostaining. HE staining images of the CCC component (**a**), the CoCC component (**d**), and the poorly differentiated CCC component (**e**). Similarly, CK7 immunostainings of the CCC component (**b**), the CoCC component (**c**), and the poorly differentiated CCC component (**f**) are shown. In the CCC components of the tumor, cancer cells showed glandular duct-like structures, and lymphocytic infiltration was observed in fibrotic regions (**a**). Immunohistochemistry showed positivity for CK7 (**b**). In the CoCC component, smaller cancer cells resembling bile-ductular cells were observed, showing antler-like proliferation pattern (**c**). Immunohistochemistry also showed positivity for CK7 (**d**). In the poorly differentiated CCC component, pleomorphic cells showed severe cellular atypia with HCC-like compact proliferation with less fibrotic region (**e**). Immunohistochemical examination showed positive for CK7 (**f**)

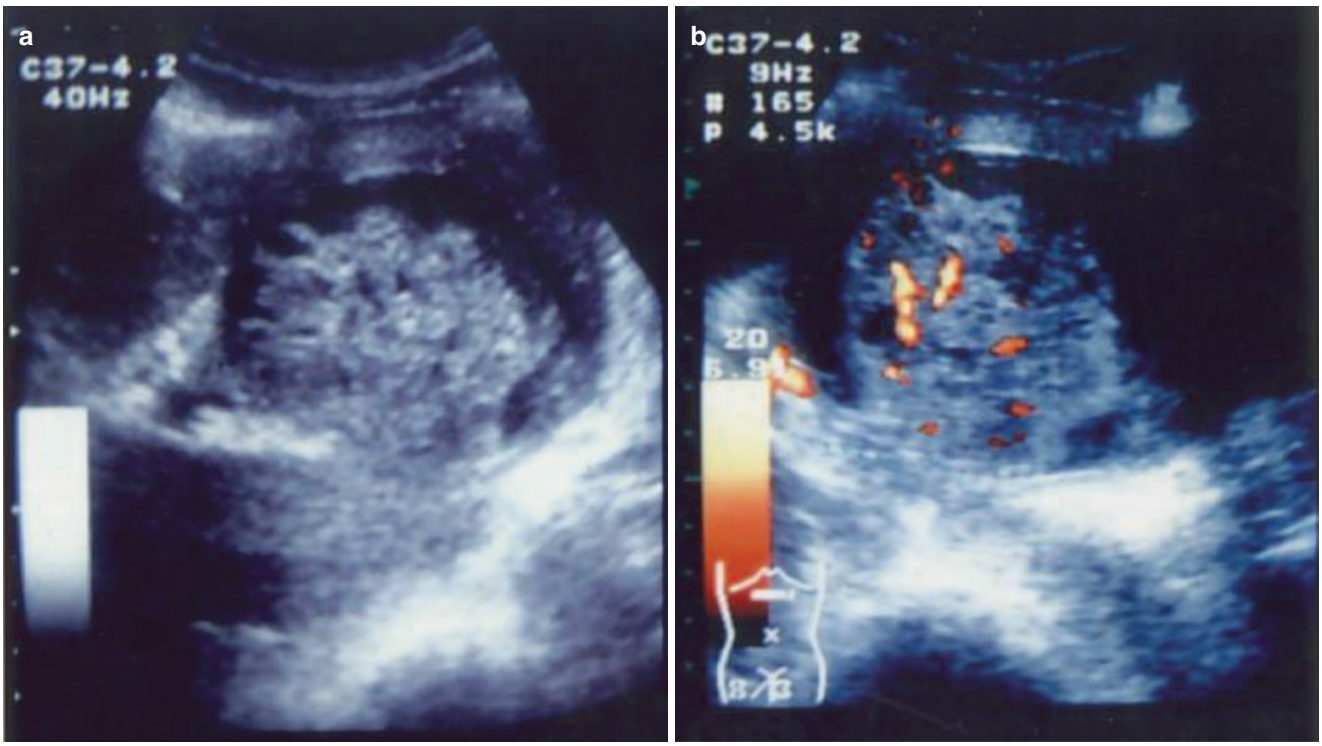

Fig. 17.30 Cystadenocarcinoma; US images. US shows a high-echoic tumor surrounded by a low-echoic area (**a**). Doppler US shows arterial flow in the tumor (**b**)

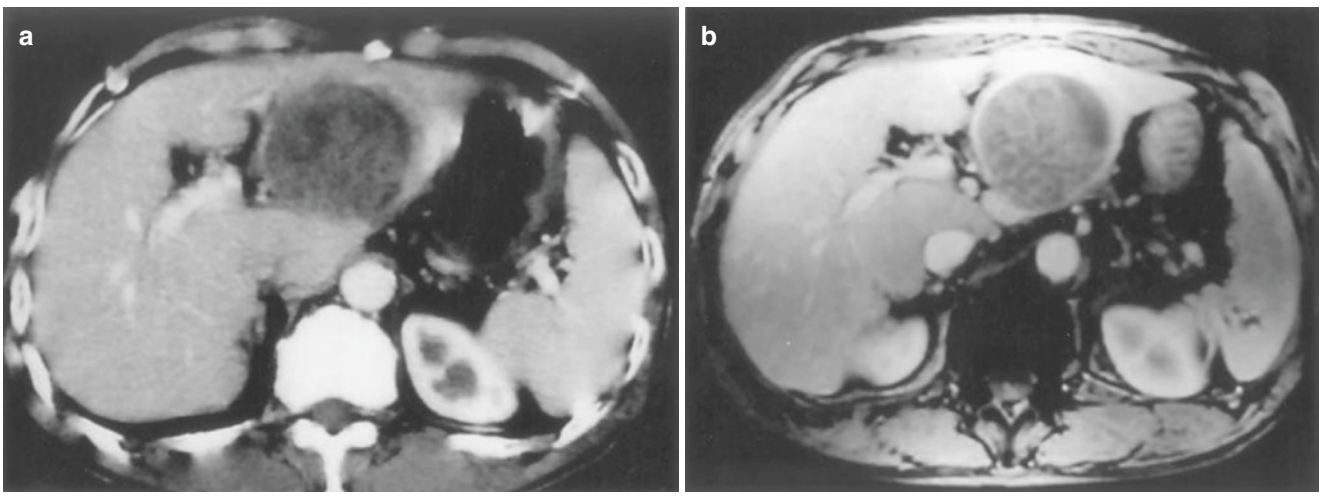

Fig. 17.31 Cystadenocarcinoma; CT images. CT in the early phase shows a low-density area in S4. There are arterial vessels in the tumor, and it is surrounded by arteries (**a**). CT in the late phase reveals low or heterogeneous density in the tumor, and there is a low-density area on edge (**b**)

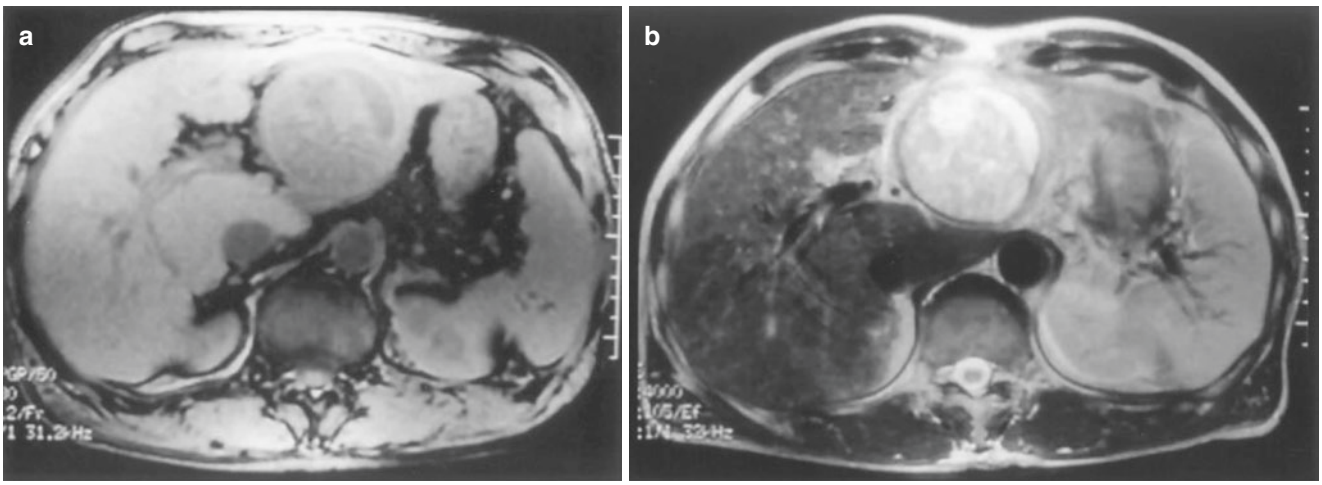

Fig. 17.32 Cystadenocarcinoma; MRI images. MRI with T1 intensification shows iso-intensity in the tumor with high intensity in its rim (**a**). MRI with T2 intensification shows high intensity in the tumor with low intensity in its rim (**b**)

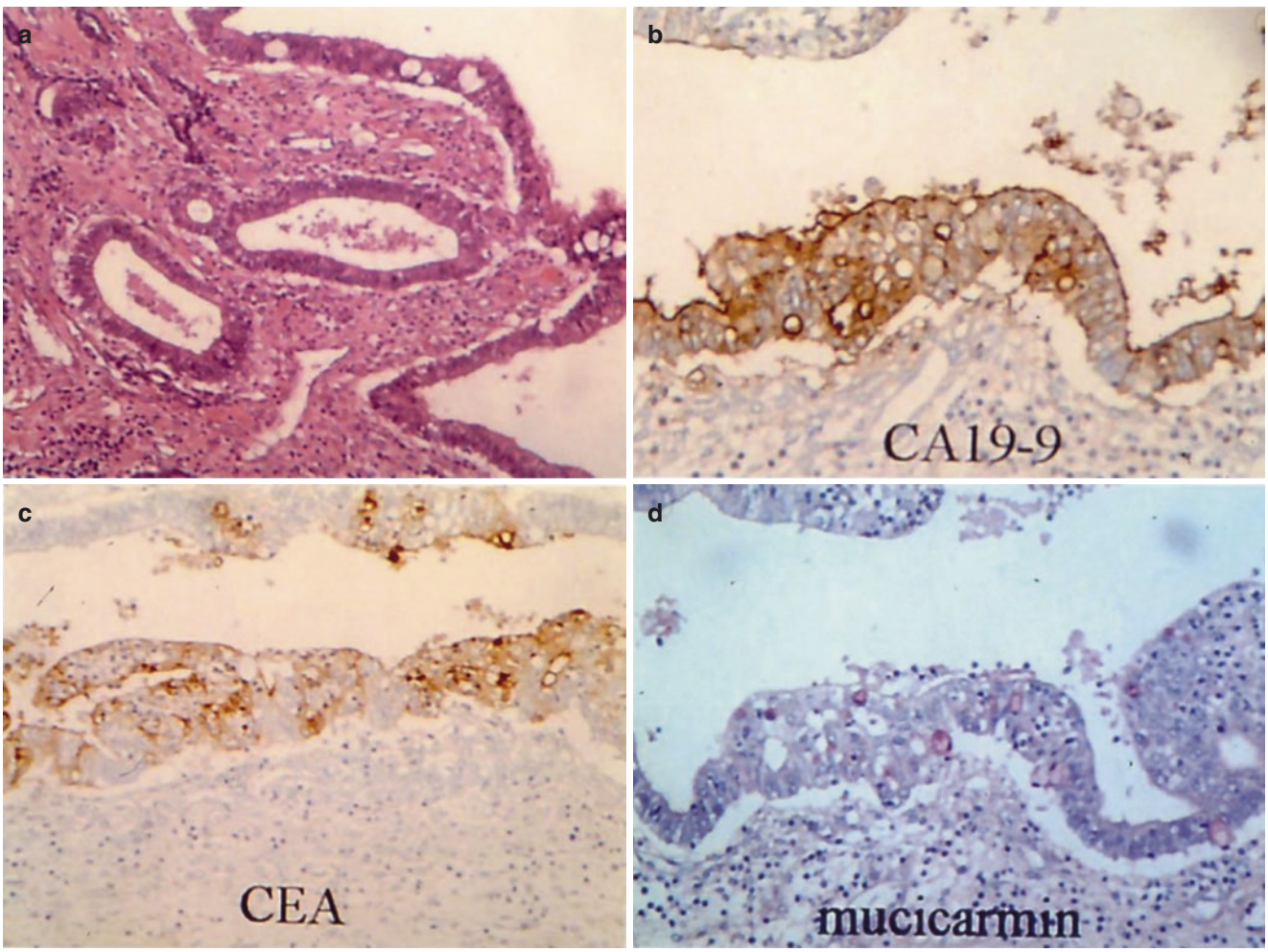

Fig. 17.33 Cystadenocarcinoma; microscopic views. Cystic areas lined by cuboidal to low columnar epithelium overlying cellular mesenchymal stroma (**a**). The tumor shows cytoplasmic and apical membranous staining for CA19-9 (**b**). Cystadenocarcinoma with membranous and cytoplasmic CEA staining. (**d**) Mucin in the epithelium of the cystadenocarcinoma is stained red with mucicarmine (**c**)

even in old-aged individuals [37]. The usual presentations are weight loss, large upper abdominal mass, and high serum AFP. Plain CT shows isodensity or low-density tumor with calcification on the periphery [38]. Histologically, there are three types of hepatoblastoma: epithelial, mixed epithelial-mesenchymal, and anaplastic [39]. Fetal hepatocytes contain more fat and glycogen than adult hepatocytes, and a pale appearance or light-and-dark pattern is seen in the fetal type of hepatoblastoma. Anaplastic type is characterized by high nuclear-cytoplasmic ratio, proliferative activity, poorly defined cellular margins, and squamous differentiation.

Case 17.9

A 5-month-old infant was admitted for an abdominal tumor. His serum AFP was as high as 61 × 10^4 ng/mL, and CT showed a low-density area with calcification in S3 to S4 (Fig. 17.34). MRI revealed low intensity in S4 on T1-weighted image and high intensity on T2-weighted image (Fig. 17.35).

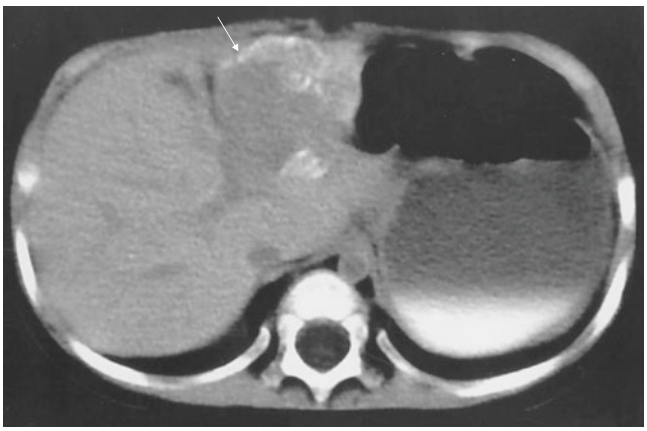

Fig. 17.34 Hepatoblastoma; CT images. A low-density tumor with calcification (arrow) is observed in S4 (medial segment) by CT

After diagnosis, the tumor was resected and showed cords of small hepatocytes (fetal epithelial type), tubular form in other areas (embryonal epithelial type), and focal keratinization (squamous differentiation) (Fig. 17.36).

Hepatomegaly and elevation of AFP in serum led to a working diagnosis of hepatoblastoma. Image analysis and liver biopsy confirm its diagnosis. Early detection may lead to curative resection. Preoperative chemotherapy reduces the size of the tumor. Surgical resection and liver transplantation need to be required [40].

17.6 Liver Sarcoma

Compared to carcinomas, sarcomas of the liver are very rare and should be differentiated from HCC.

17.7 Epithelioid Hemangioendothelioma

Endothelial tumor in the lung may present as primary liver tumor, and its prognosis varies widely. Some patients survive for decades, while others die within months. Its causes are unknown. A relationship to the use of oral contraceptive is postulated [41], and women are more often affected than men.

Case 17.10

A 44-year-old female with a history of oral contraceptive use presented with space-occupying lesions in the liver. CECT showed multiple tumors in the peripheral of S2, S4, S5, and S6 in the early phase (Fig. 17.37). Resected liver showed distribution of tumor cells and stroma in the periportal area, distribution of individual tumor cells in fibrous stroma, formation of vasculature from tumor cells, and

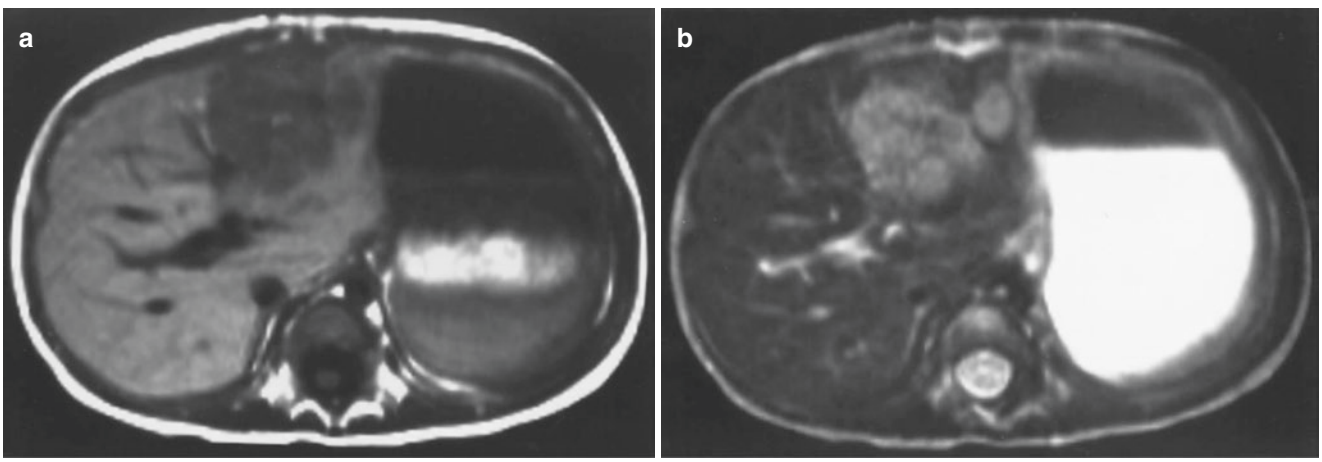

Fig. 17.35 Hepatoblastoma; MRI images. MRI shows low-intensity lesion with a calcified rim (**a**). MRI with T2 intensification reveals a high-intensity area in S4 (**b**)

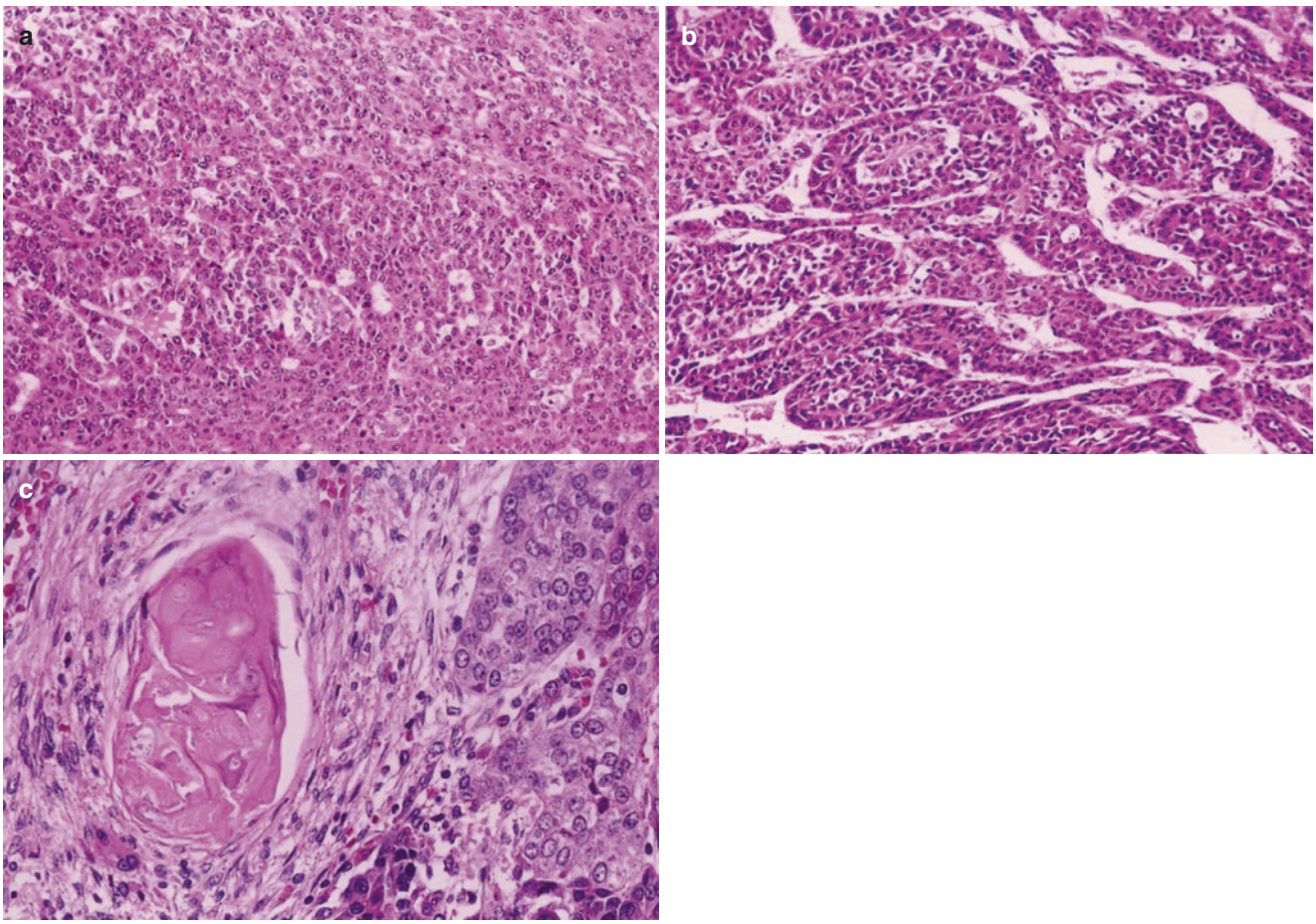

Fig. 17.36 Hepatoblastoma; histological view. (**a**) Hepatoblastoma, fetal epithelial type. The tumor is composed of sheets and thin trabeculae of small hepatocytes. (**b**) Hepatoblastoma, embryonal epithelial type. The tumor cells have a high nuclear-cytoplasmic ratio and are arranged in glandular pattern. (**c**) Hepatoblastoma. There is keratinization formation in hepatoblastoma

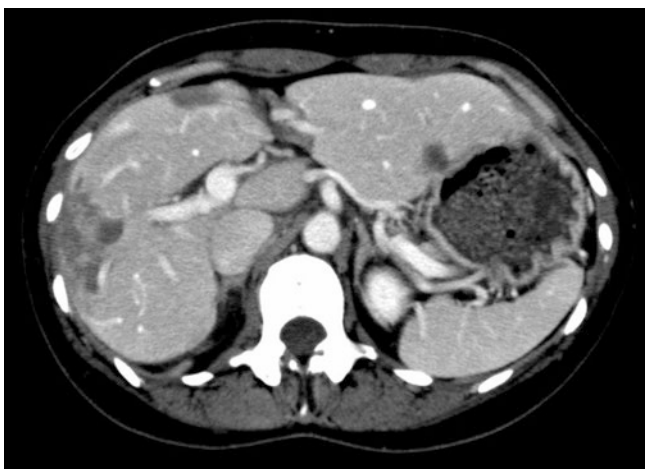

Fig. 17.37 Epithelioid hemangioendothelioma; CT images. CECT shows multiple low-density areas in the early phase, and these are localized mainly in the periphery of the liver. (Courtesy of Professor H Haga)

CD34 immunoreactivity in the tumor cells (Fig. 17.38). The tumor grows slowly but may metastasize [42]. Liver transplantation pertains to a favorable 5-year survival rate [43].

17.8 Angiosarcoma

Although it accounts for only 1–2% of primary hepatic malignancies, angiosarcoma is the most common sarcoma of the liver [44]. There are known predisposing factors, such as exposure to thorium (Thorotrast), vinyl chloride, and arsenic [44]. The incubation period is long from 15 to 25 years. Steroid hormones and urethane are also associated with the development of angiosarcoma [45, 46]. Symptoms and signs include pain, anemia, fever of unknown origin, weight loss, abdominal mass, and hemoperitoneum. The median survival is 6 months. Although imaging studies are helpful, they are inconclusive. Hence, liver biopsy is often required under peritoneoscopy.

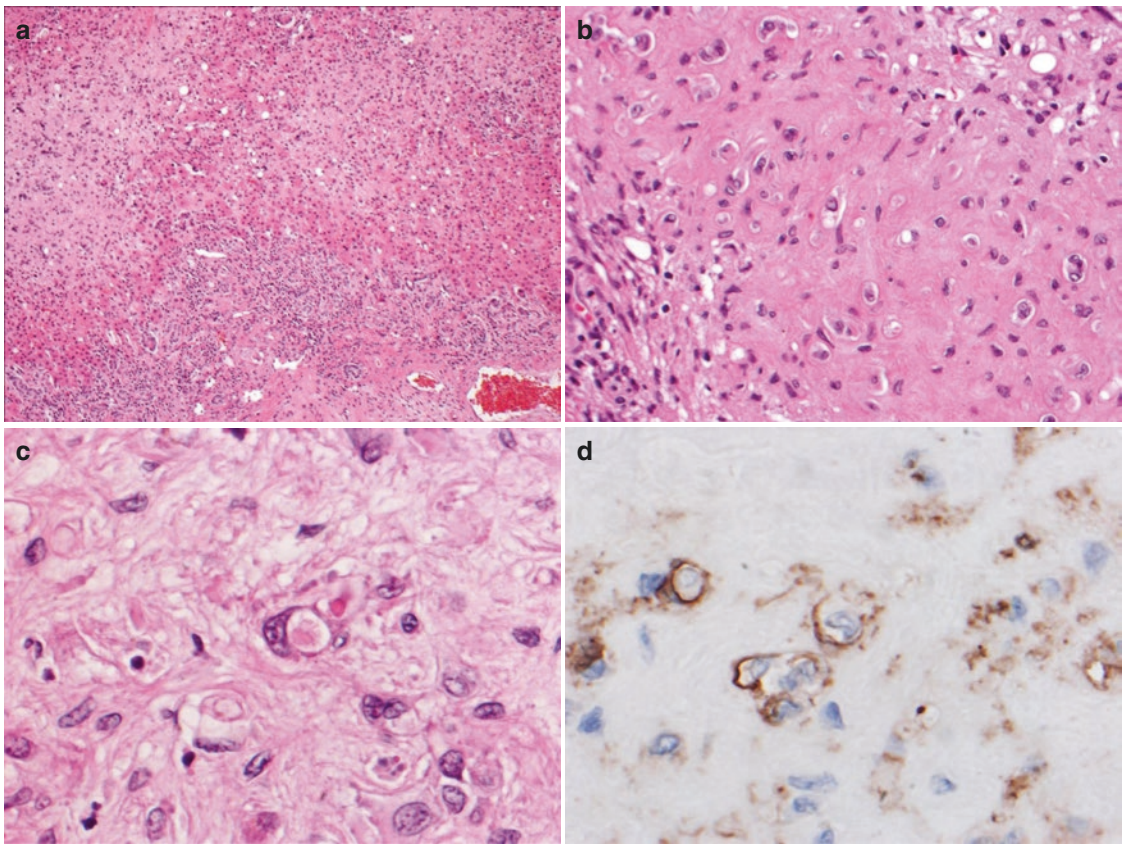

Fig. 17.38 Epithelioid hemangioendothelioma; microscopic views. Glandular structures of tumor cells are distributed in the periportal tract (**a**). Tumor cells are mixed with fibrosis (**b**). Tumor cells form a capillary structure (signet ringlike tumor cell) (**c**). CD34 immunoreactivity is seen in tumor cells (**d**). (Courtesy of Professor H Haga)

Case 17.11

A 47-year-old male presented with weight loss and a history of diabetes mellitus for 5 years. There were no predisposing factors, such as Thorotrast or vinyl chloride. His laboratory data showed T-BIL 1.9 mg/dL, AST 83 IU/L, ALT 111 IU/L, ALP 777 IU/L, LAP 1340 IU/L, GGT 3490 IU/L, FBS 191 mg/dL, AFP 2 ng/mL, $ICGR_{15}$ 56%, and PLT 9.6×10^4. US revealed many small tumors in the liver (Fig. 17.39). Plain CT presented heterogeneous tumor, and CECT did not reveal different densities (Fig. 17.40). Peritoneoscopy showed red nodules with prominence of the undersurface of the liver (Fig. 17.41). Angiography showed multiple staining with portal vein obstruction by a tumor thrombus (Fig. 17.42). He soon complained of epigastric pain and ascites and died of liver rupture.

Autopsy tissue revealed irregularly dilated sinusoids and congestion. The sinusoids were lined by atypical and multinucleated endothelial cells, which are in multiple layers, as well as compressed hepatocytes. Immunohistochemistry showed factor VIII in atypical endothelial cells (Fig. 17.43).

The tumor progresses quickly and grows multicentrically. Metastases occur in the lung, hilar lymph node, spleen, and bone. A sudden complication is rupture with hemoperitoneum; the course is progressive, and the prognosis is poor.

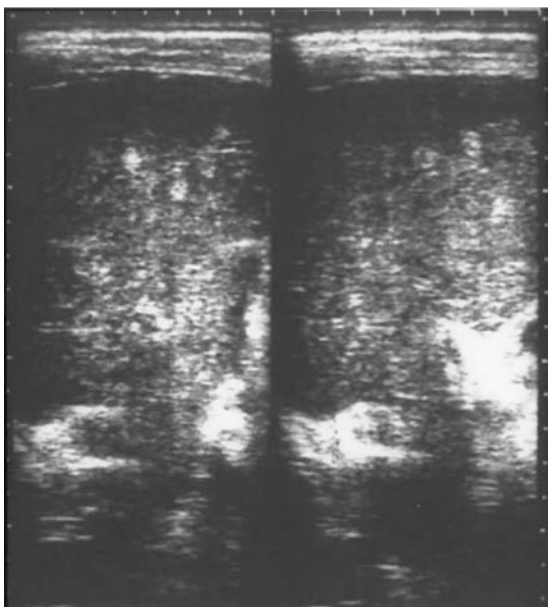

Fig. 17.39 Angiosarcoma; US images. US shows multiple high and small echogenic lesions in the liver. The figures of this case are courtesy of Dr. Maki Iwai, Kyoto Prefectural University of Medicine and (Reuse of Iwai M, et al. A case report of primary hepatic angiosarcoma. J Kyoto Pref Univ Med 1988; 97: 859–68, with permission of its chief editor)

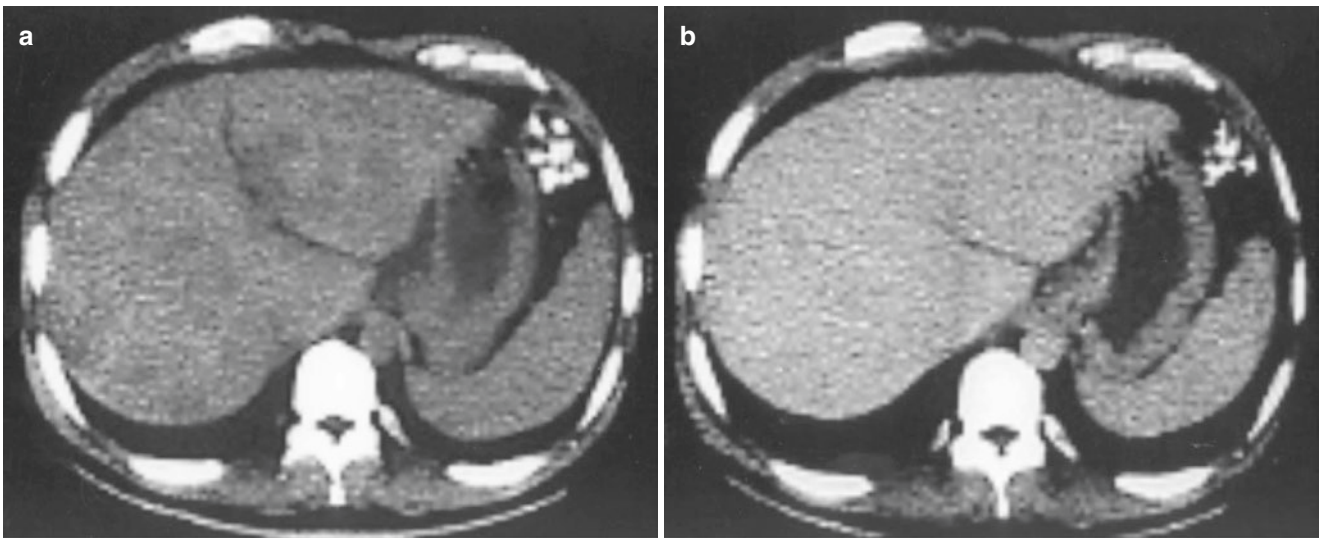

Fig. 17.40 Angiosarcoma; CT images. Plain CT shows heterogeneous density in the liver (**a**). CECT shows homogenous density in the liver (**b**). (Reuse of Iwai M, et al. A case report of primary hepatic angiosarcoma. J Kyoto Pref Univ Med 1988; 97: 859–68, with permission of its chief editor)

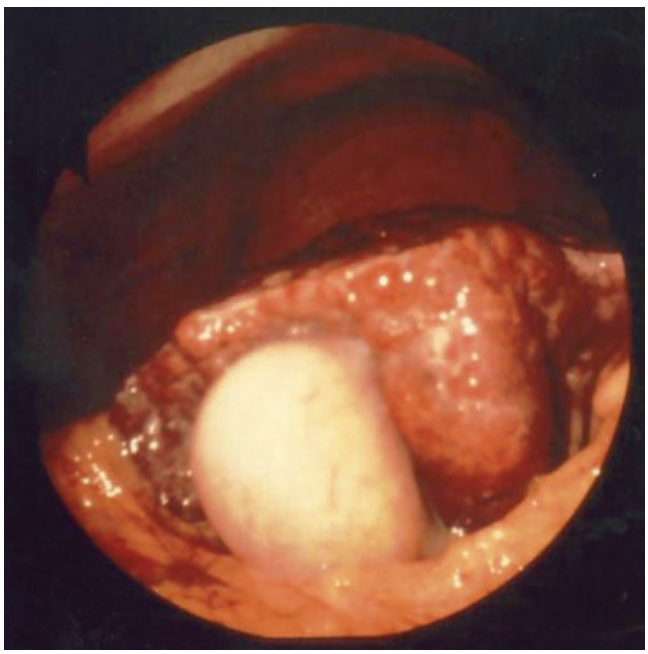

Fig. 17.41 Angiosarcoma; peritoneoscopy. Peritoneoscopy shows an irregular surface of the liver and protrusion of the undersurface in the inner area of the gallbladder. There is nodular formation on the surface, and the nodular surface is red in color and hypervascular. (Reuse of Iwai M, et al. A case report of primary hepatic angiosarcoma. J Kyoto Pref Univ Med 1988; 97: 859–68, with permission of its chief editor)

17.9 Primary Hepatic Neuroendocrine Tumor

A neuroendocrine neoplasm (NEN) derives from neuroendocrine cells which are present throughout the body in various organs such as the lungs and gastrointestinal tract. NEN is histologically classified based on morphology, Ki-67 index, and mitotic count. Neuroendocrine tumor (NET) G1 shows Ki-67 index ≤2%, NET G2 represents Ki-67 index = 3–20%, and neuroendocrine cancer (NEC) shows Ki-67 index >20%. NET is a slow-growing tumor; NEC is aggressive [47]. Primary hepatic neuroendocrine tumor is extremely rare.

Case 17.12

A 75-year-old female was pointed out approximately 20 mm hepatic tumor localized in S4 on CT. The results for blood routines, liver function, and tumor marker were within normal ranges. The tumor showed ring enhancement in the arterial phase (Fig. 17.44) and delayed enhancement on the central part of tumor. Similarly, CEUS also revealed ring enhancement accompanied by the delayed enhancement and defect in the post-vascular phase (Fig. 17.44). Resected liver tissues showed the distribution of tumor cells accompanied by fibrovascular stroma and pseudo-ductal structures (Fig. 17.45). The central part of the tumor was associated with hemorrhagic necrosis and edematous degeneration. Immunohistochemistry findings included chromogranin A (+), synaptophysin (+), CD56 (+), CDX2 (+), mucicarmine (−), CEA (−), cytokeratin7 (−), cytokeratin20 (−), and estrogen receptor (−) (Fig. 17.45). Ki-67 (MIB-1) index was less than 2%. Because no primary organ was found in postoperative examination, the tumor was considered as a primary neuroendocrine tumor of the liver (G1).

Acknowledgment We are grateful to Prof. Alex Y. Chang for constructive advice for first edition of this chapter.

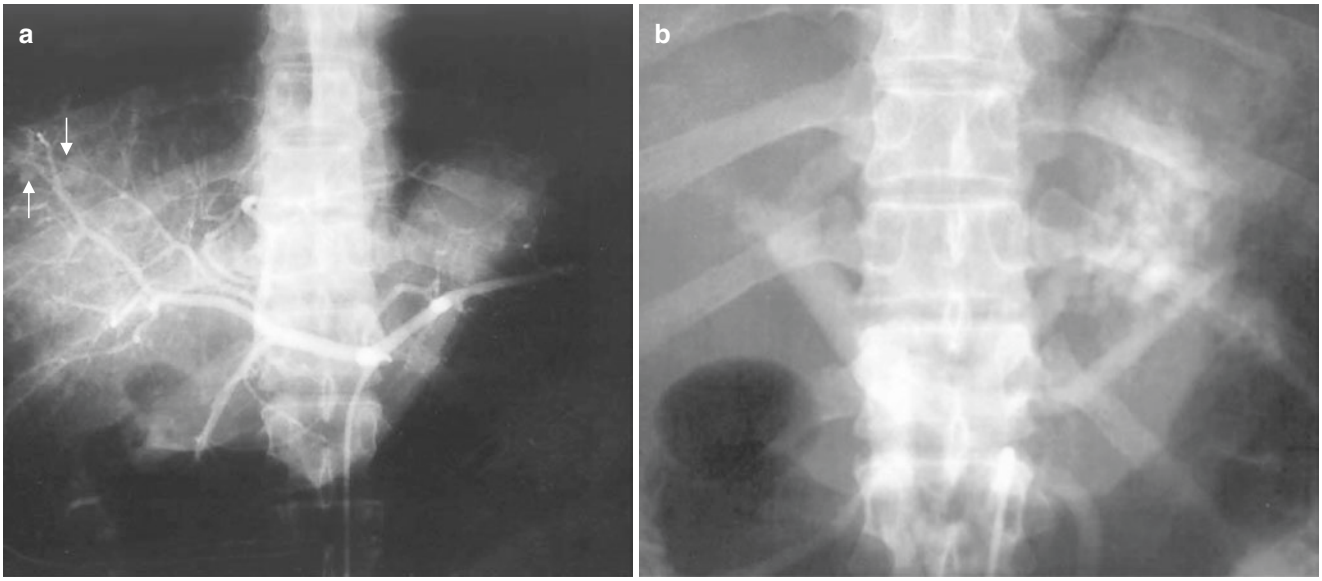

Fig. 17.42 Angiosarcoma; angiography. Angiography shows multiple small tumor staining (arrow) in the right lobe (**a**). Portography reveals tumor thrombus in portal trunk (**b**). (Reuse of Iwai M, et al. A case report of primary hepatic angiosarcoma. J Kyoto Pref Univ Med 1988; 97: 859–68, with permission of its chief editor)

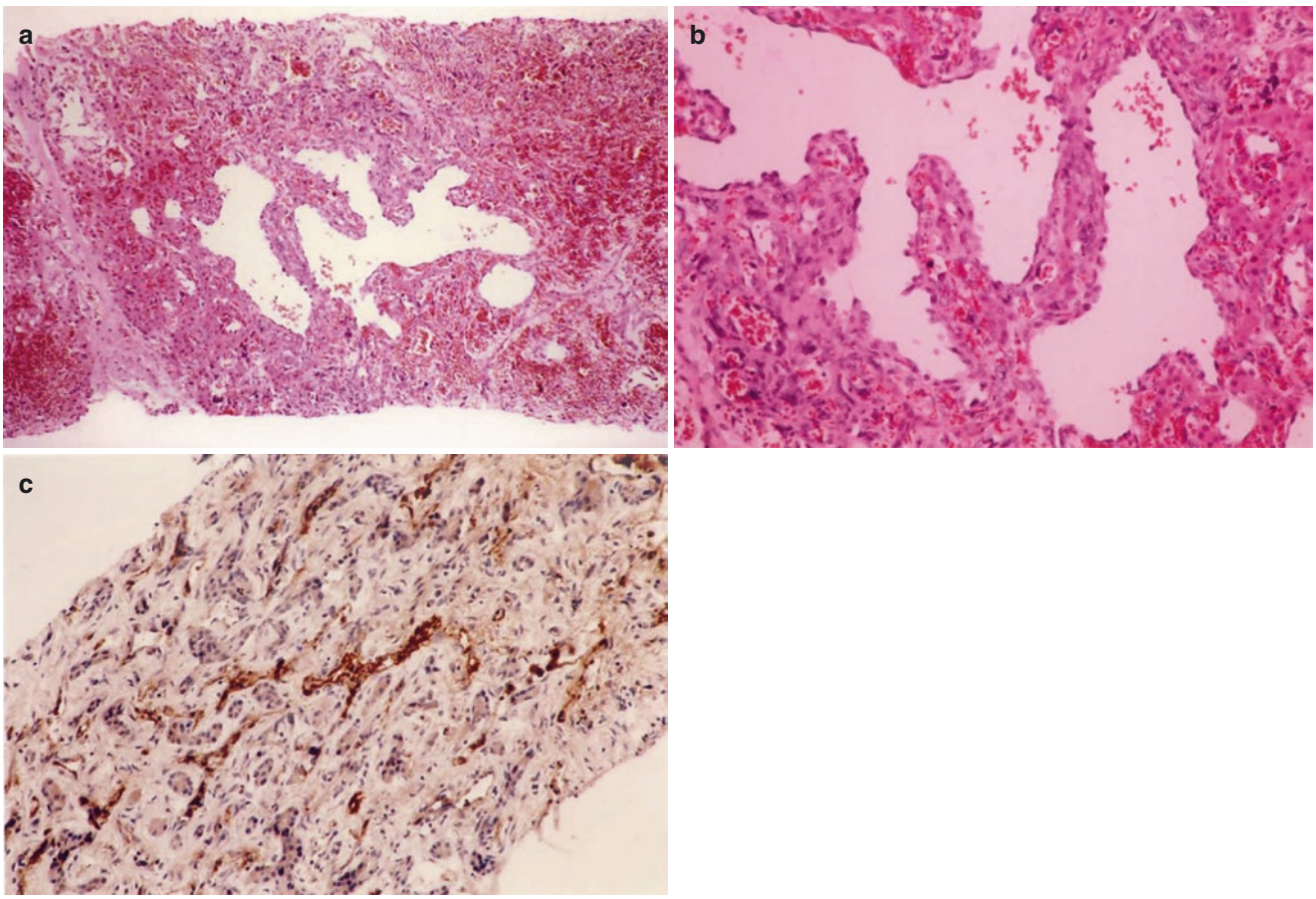

Fig. 17.43 Angiosarcoma; microscopic views. Irregularly dilated sinusoids and congestion are seen (**a**). The tumor shows cavernous sinusoids lined with pleomorphic and hyperchromatic endothelial cells. Hepatocytes are not seen (**b**). Immunostaining reveals that the tumor cells are focally positive for factor VIII (**c**). (Reuse of Iwai M, et al. A case report of primary hepatic angiosarcoma. J Kyoto Pref Univ Med 1988; 97: 859–68, with permission of its chief editor)

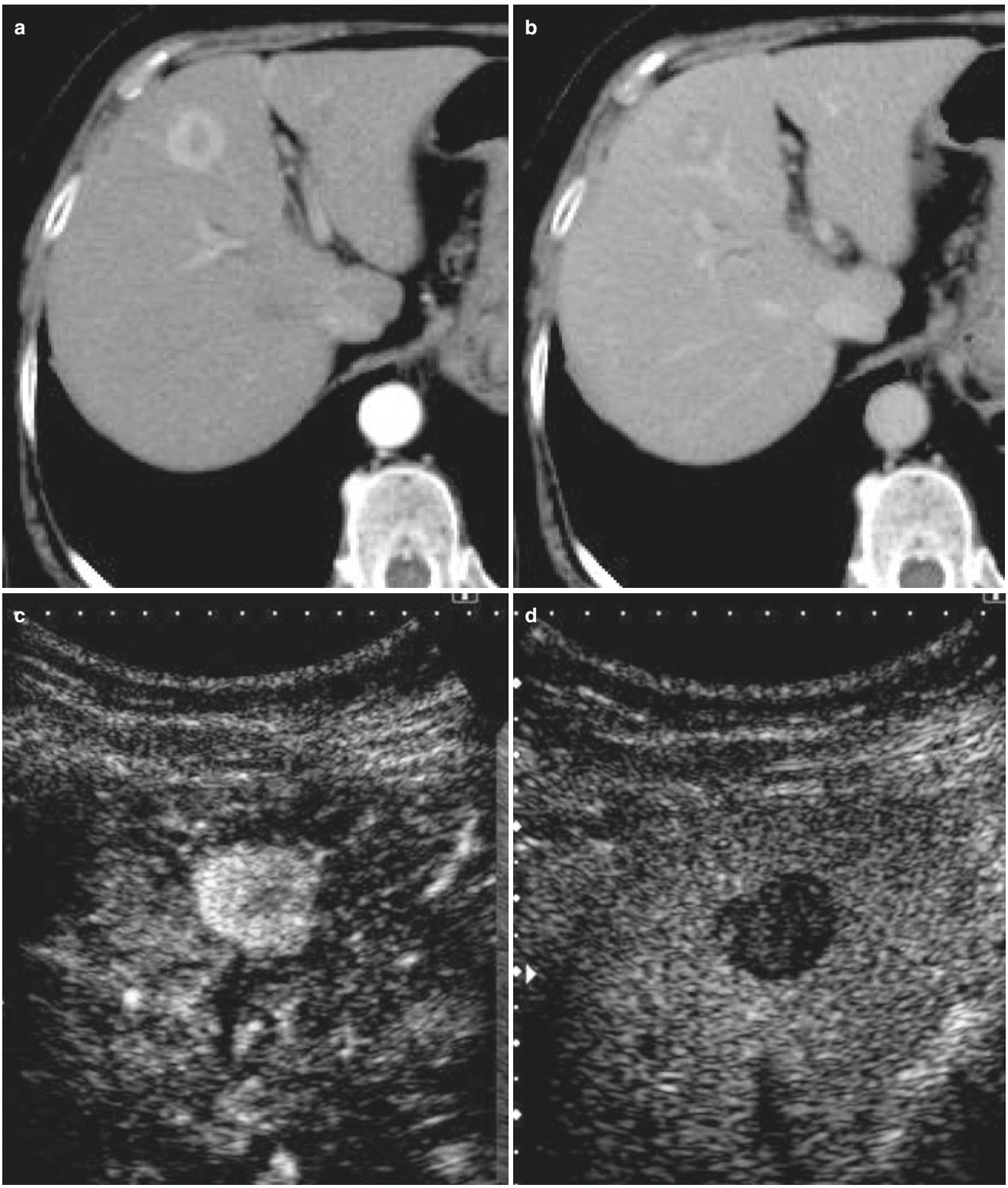

Fig. 17.44 Primary hepatic neuroendocrine tumor. CECT showed ring enhancement in the arterial phase (**a**) and delayed enhancement on the central part of tumor in the equilibrium phase (**b**). CEUS showed ring enhancement with delayed enhancement on the central part in the vascular phase (**c**) and complete defect in the post-vascular phase (**d**)

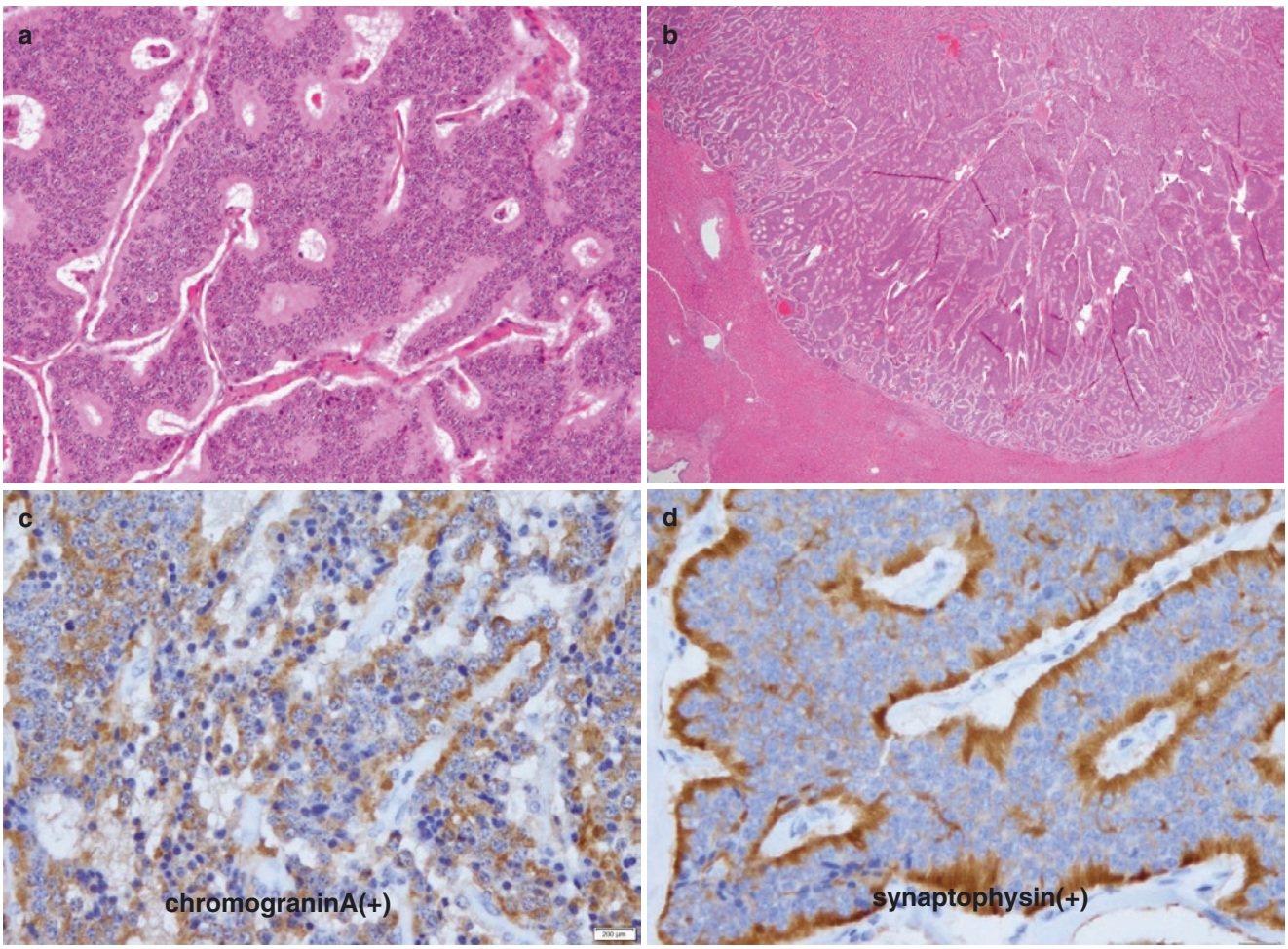

Fig. 17.45 Primary hepatic neuroendocrine tumor; microscopic views. Pathological findings showed the distribution of tumor cells accompanied by fibrovascular stroma and pseudo-ductal structures (**a**) and hemorrhagic necrosis and edematous degeneration in the central part of the tumor (**b**). Immunostaining findings of chromogranin A (**c**) and synaptophysin (**d**) are shown

References

1. Lai CL, Yuen MF. Prevention of hepatitis B virus-related hepatocellular carcinoma with antiviral therapy. Hepatology. 2013;57:399–408.
2. Morgan RL, Baack B, Smith BD, Yartel A, Pitasi M, Falck-Ytter Y. Eradication of hepatitis C virus infection and the development of hepatocellular carcinoma: a meta-analysis of observational studies. Ann Intern Med. 2013;158:329–37.
3. Idilman R, De Maria N, Colantoni A, Van Thiel DH. Pathogenesis of hepatitis B and C-induced hepatocellular carcinoma. J Viral Hepat. 1998;5:285–99.
4. Wogan GN. Aflatoxins as risk factors for hepatocellular carcinoma in humans. Cancer Res. 1992;52:2114s–8s.
5. International Consensus Group for Hepatocellular Neoplasia. Pathologic diagnosis of early hepatocellular carcinoma: a report of the international consensus group for hepatocellular neoplasia. Hepatology. 2009;49:658–64.
6. Peng SY, Lai PL, Chu JS, Lee PH, Tsung PT, Chen DS, Hsu HC. Expression and hypomethylation of alpha-fetoprotein gene in unicentric and multicentric human hepatocellular carcinomas. Hepatology. 1993;17:35–41.
7. Aoyagi Y, Saitoh A, Suzuki Y, Igarashi K, Oguro M, Yokota T, Mori S, et al. Fucosylation index of alpha-fetoprotein, a possible aid in the early recognition of hepatocellular carcinoma in patients with cirrhosis. Hepatology. 1993;17:50–2.
8. Okuda H, Nakanishi T, Takatsu K, Saito A, Hayashi N, Takasaki K, Takenami K, et al. Serum levels of des-gamma-carboxy prothrombin measured using the revised enzyme immunoassay kit with increased sensitivity in relation to clinicopathologic features of solitary hepatocellular carcinoma. Cancer. 2000;88:544–9.
9. Bottelli R, Tibballs J, Hochhauser D, Watkinson A, Dick R, Burroughs AK. Ultrasound screening for hepatocellular carcinoma (HCC) in cirrhosis: the evidence for an established clinical practice. Clin Radiol. 1998;53:713–6.
10. Kim CK, Lim JH, Lee WJ. Detection of hepatocellular carcinomas and dysplastic nodules in cirrhotic liver: accuracy of ultrasonography in transplant patients. J Ultrasound Med. 2001;20:99–104.
11. Kudo M. The 2008 Okuda lecture: management of hepatocellular carcinoma: from surveillance to molecular targeted therapy. J Gastroenterol Hepatol. 2010;25:439–52.
12. Kuszyk BS, Bluemke DA, Urban BA, Choti MA, Hruban RH, Sitzmann JV, Fishman EK. Portal-phase contrast-enhanced helical

CT for the detection of malignant hepatic tumors: sensitivity based on comparison with intraoperative and pathologic findings. AJR Am J Roentgenol. 1996;166:91–5.
13. Ward J, Guthrie JA, Scott DJ, Atchley J, Wilson D, Davies MH, Wyatt JI, et al. Hepatocellular carcinoma in the cirrhotic liver: double-contrast MR imaging for diagnosis. Radiology. 2000;216:154–62.
14. Forner A, Llovet JM, Bruix J. Hepatocellular carcinoma. Lancet. 2012;379:1245–55.
15. Vilgrain V, Van Beers BE, Pastor CM. Insights into the diagnosis of hepatocellular carcinomas with hepatobiliary MRI. J Hepatol. 2016;64:708–16.
16. Bruix J, Reig M, Sherman M. Evidence-based diagnosis, staging, and treatment of patients with hepatocellular carcinoma. Gastroenterology. 2016;150:835–53.
17. Llovet JM, Ricci S, Mazzaferro V, Hilgard P, Gane E, Blanc JF, de Oliveira AC, et al. Sorafenib in advanced hepatocellular carcinoma. N Engl J Med. 2008;359:378–90.
18. Bruix J, Qin S, Merle P, Granito A, Huang YH, Bodoky G, Pracht M, et al. Regorafenib for patients with hepatocellular carcinoma who progressed on sorafenib treatment (RESORCE): a randomised, double-blind, placebo-controlled, phase 3 trial. Lancet. 2017;389:56–66.
19. Kudo M, Finn RS, Qin S, Han KH, Ikeda K, Piscaglia F, Baron A, et al. Lenvatinib versus sorafenib in first-line treatment of patients with unresectable hepatocellular carcinoma: a randomised phase 3 non-inferiority trial. Lancet. 2018;391:1163–73.
20. Ishii H, Okada S, Okusaka T, Yoshimori M, Nakasuka H, Shimada K, Yamasaki S, et al. Needle tract implantation of hepatocellular carcinoma after percutaneous ethanol injection. Cancer. 1998;82:1638–42.
21. Kudo M. A new era of systemic therapy for hepatocellular carcinoma with regorafenib and lenvatinib. Liver Cancer. 2017;6:177–84.
22. Razumilava N, Gores GJ. Cholangiocarcinoma. Lancet. 2014;383:2168–79.
23. Shiota K, Taguchi J, Nakashima O, Nakashima M, Kojiro M. Clinicopathologic study on cholangiolocellular carcinoma. Oncol Rep. 2001;8:263–8.
24. Theise ND, Yao JL, Harada K, Hytiroglou P, Portmann B, Thung SN, Tsui W, et al. Hepatic 'stem cell' malignancies in adults: four cases. Histopathology. 2003;43:263–71.
25. Brunt E, Aishima S, Clavien PA, Fowler K, Goodman Z, Gores G, Gouw A, et al. cHCC-CCA: consensus terminology for primary liver carcinomas with both hepatocytic and cholangiocytic differentiation. Hepatology. 2018;68(1):113–26.
26. Okuda K, Nakanuma Y, Miyazaki M. Cholangiocarcinoma: recent progress. Part 1: epidemiology and etiology. J Gastroenterol Hepatol. 2002;17:1049–55.
27. Koga A, Ichimiya H, Yamaguchi K, Miyazaki K, Nakayama F. Hepatolithiasis associated with cholangiocarcinoma. Possible etiologic significance. Cancer. 1985;55:2826–9.
28. Bloustein PA. Association of carcinoma with congenital cystic conditions of the liver and bile ducts. Am J Gastroenterol. 1977;67:40–6.
29. Shaib Y, El-Serag HB. The epidemiology of cholangiocarcinoma. Semin Liver Dis. 2004;24:115–25.
30. Jusakul A, Cutcutache I, Yong CH, Lim JQ, Huang MN, Padmanabhan N, Nellore V, et al. Whole-genome and epigenomic landscapes of etiologically distinct subtypes of cholangiocarcinoma. Cancer Discov. 2017;7:1116–35.
31. Nakamura H, Arai Y, Totoki Y, Shirota T, Elzawahry A, Kato M, Hama N, et al. Genomic spectra of biliary tract cancer. Nat Genet. 2015;47:1003–10.
32. Nakanuma Y, Miyata T, Uchida T. Latest advances in the pathological understanding of cholangiocarcinomas. Expert Rev Gastroenterol Hepatol. 2016;10:113–27.
33. Bridgewater J, Galle PR, Khan SA, Llovet JM, Park JW, Patel T, Pawlik TM, et al. Guidelines for the diagnosis and management of intrahepatic cholangiocarcinoma. J Hepatol. 2014;60:1268–89.
34. Akwari OE, Tucker A, Seigler HF, Itani KM. Hepatobiliary cystadenoma with mesenchymal stroma. Ann Surg. 1990;211:18–27.
35. Vachha B, Sun MR, Siewert B, Eisenberg RL. Cystic lesions of the liver. AJR Am J Roentgenol. 2011;196:W355–66.
36. Shrikhande S, Kleeff J, Adyanthaya K, Zimmermann A, Shrikhande V. Management of hepatobiliary cystadenocarcinoma. Dig Surg. 2003;20:60–3.
37. Bortolasi L, Marchiori L, Dal Dosso I, Colombari R, Nicoli N. Hepatoblastoma in adult age: a report of two cases. Hepatogastroenterology. 1996;43:1073–8.
38. King SJ, Babyn PS, Greenberg ML, Phillips MJ, Filler RM. Value of CT in determining the resectability of hepatoblastoma before and after chemotherapy. AJR Am J Roentgenol. 1993;160:793–8.
39. Gonzalez-Crussi F, Upton MP, Maurer HS. Hepatoblastoma. Attempt at characterization of histologic subtypes. Am J Surg Pathol. 1982;6:599–612.
40. Kremer N, Walther AE, Tiao GM. Management of hepatoblastoma: an update. Curr Opin Pediatr. 2014;26:362–9.
41. Malamut G, Perlemuter G, Buffet C, Bedossa P, Joly JP, Colombat M, Kuoch V, et al. [Epithelioid hemangioendothelioma associated with nodular regenerative hyperplasia]. Gastroenterol Clin Biol. 2001;25:1105–7.
42. Demetris AJ, Minervini M, Raikow RB, Lee RG. Hepatic epithelioid hemangioendothelioma: biological questions based on pattern of recurrence in an allograft and tumor immunophenotype. Am J Surg Pathol. 1997;21:263–70.
43. Kayler LK, Merion RM, Arenas JD, Magee JC, Campbell DA, Rudich SM, Punch JD. Epithelioid hemangioendothelioma of the liver disseminated to the peritoneum treated with liver transplantation and interferon alpha-2B. Transplantation. 2002;74:128–30.
44. Chaudhary P, Bhadana U, Singh RA, Ahuja A. Primary hepatic angiosarcoma. Eur J Surg Oncol. 2015;41:1137–43.
45. Falk H, Thomas LB, Popper H, Ishak KG. Hepatic angiosarcoma associated with androgenic-anabolic steroids. Lancet. 1979;2:1120–3.
46. Cadranel JF, Legendre C, Desaint B, Delamarre N, Florent C, Levy VG. Liver disease from surreptitious administration of urethane. J Clin Gastroenterol. 1993;17:52–6.
47. Rindi G, Petrone G, Inzani F. The 2010 WHO classification of digestive neuroendocrine neoplasms: a critical appraisal four years after its introduction. Endocr Pathol. 2014;25:186–92.